Geophys. J. R. astr. Soc. (1974) **36**, 541–576.

Numerical Modelling of Instantaneous Plate Tectonics*

J. B. Minster, T. H. Jordan, P. Molnar and E. Haines

(Received 1973 September 19)†

Summary

Assuming lithospheric plates to be rigid, we systematically invert 68 spreading rates, 62 fracture zones trends and 106 earthquake slip vectors simultaneously to obtain a self-consistent model of instantaneous relative motions for eleven major plates. The inverse problem is linearized and solved iteratively by a maximum likelihood procedure. Because the uncertainties in the data are small, Gaussian statistics are shown to be adequate. The use of a linear theory permits (1) the calculation of the uncertainties in the various angular velocity vectors caused by uncertainties in the data, and (2) quantitative examination of the distribution of information within the data set.

The existence of a self-consistent model satisfying all the data is strong justification of the rigid plate assumption. Slow movement between North and South America is shown to be resolvable.

We then invert the trends of 20 linear island chains and aseismic ridges under the assumptions that they represent the directions of plate motions over a set of hot spots fixed with respect to each other. We conclude that these hot spots have had no significant relative motions in the last 10 My.

1. Introduction

One aspect of plate tectonics that helped establish it as a viable theory is the predictive capability that it offers: by knowing the relative motions of rigid plates in one region, one can deduce what they are elsewhere. Clearly, the more accurately we know the relative motions in areas where there are data, the more reliable will our predictions be in other regions. Nevertheless we are limited to studying relative motions, and there remains the ambiguity of the fixed reference frame, if a physically meaningful one exists, with respect to which the plates move.

Wilson (1963, 1965) suggested that linear island chains and aseismic ridges are the surface expression of zones of upwelling in the mantle. Dietz & Holden (1970) and Morgan (1971, 1972a, b) proposed further that these hot spots are fixed with respect to one another, and constitute a possible reference frame, probably fixed with respect to the lower mantle.

A crucial test of this idea is to rotate the various plates back to their relative positions at various times in the past, and to compare the known locations and ages

* Contribution No. 2274, Division of Geological and Planetary Sciences, California Institute of Technology, Pasadena, California 91109.

† Received in original form 1973 June 13.

of the volcanic islands and aseismic ridges with those predicted by this hypothesis. The analysis would involve finite rotations for all the plates, and at present the data are not adequate for a complete study, but a first step is possible. Instantaneous rotation vectors are probably representative of the motion for the last 10 My in most regions. The directions of motion of the plates with respect to the various hot spots may be compared with those predicted by the known instantaneous relative motions by fixing the motion of one plate. Strong disagreement would cast serious doubt as to whether hot spots could be fixed with respect to each other, agreement would call for a more complete investigation.

Unfortunately many different angular velocities have been suggested for many of the various pairs of plates, and because of this lack of consistency, such models are inadequate to test the fixed hot spots idea. For a rigid plate model, the sum of the relative instantaneous rotation vectors between the plates crossed by any closed circuit on the Earth's surface is zero (e.g. McKenzie & Parker 1967). This closure condition can be used to determine the relative motion at plate boundaries where there are no data. Early global models were obtained by evaluating relative angular velocity vectors for the pairs of plates for which data were available. Often, however, the closure condition applied to different circuits did not yield consistent answers (e.g. Hey *et al.* 1972). In this paper we will consider the following question: Can we construct a global, self-consistent model of instantaneous rotations of rigid plates which will satisfy simultaneously all the available relative motion data? Chase (1972) presented a relative motion model obtained by an iterative least squares method. In the present paper we develop the mathematics to determine such a model, and then calculate it. This new model provides a starting point from which to construct back in time the relative motions of the plates and is the best model against which new data can be compared. Moreover with this improved kinematic model we show that the available data are consistent with the idea that the hot spots are fixed with respect to each other and form a reference frame for instantaneous motions.

Since Le Pichon (1968) calculated the relative motions of the six major plates of lithosphere, a great deal of new and better data has become available. Several thorough studies of magnetic anomalies and bathymetry in specific regions have allowed improved calculations of the relative motions of the plates involved. In addition, the determination of many new fault plane solutions, particularly at convergent plate boundaries provides a vast data set that has barely been used for plate motion studies.

We have adapted in this study the linear theory of maximum likelihood to the problem of instantaneous plate tectonics, and using this procedure, have obtained a good fit to a large data set. The procedure involves iterative improvement upon a chosen starting model until some convergence criterion is met. The maximum likelihood technique permits a full use of the uncertainty in the data; poorly determined data are weighted less than the better known ones. In addition, use of a linear theory allows us to obtain an estimate of the uncertainty attached to the model induced by the errors in the data. We have also developed further the concept of the information matrix (e.g. Wiggins 1972), using the theory of orthogonal projection operators. This allows us to evaluate the constraints imposed by self-consistency and to single out the critical plate boundaries and the important data.

The problem is non-linear, and this raises the possibility of local minima (McKenzie, Davies & Molnar 1970; Chase 1972). This question was considered with care, and a detailed discussion is found in Section 4. But as is usual in such cases, the proximity of the final model to the starting model constitutes the strongest justification for the use of a linear theory.

The basic assumption is that the plates are rigid. That all the data can be satisfactorily explained by a rigid plate model argues in favour of this premise. Of course there are complications: some plate boundaries are diffuse, such as in the Mediter-

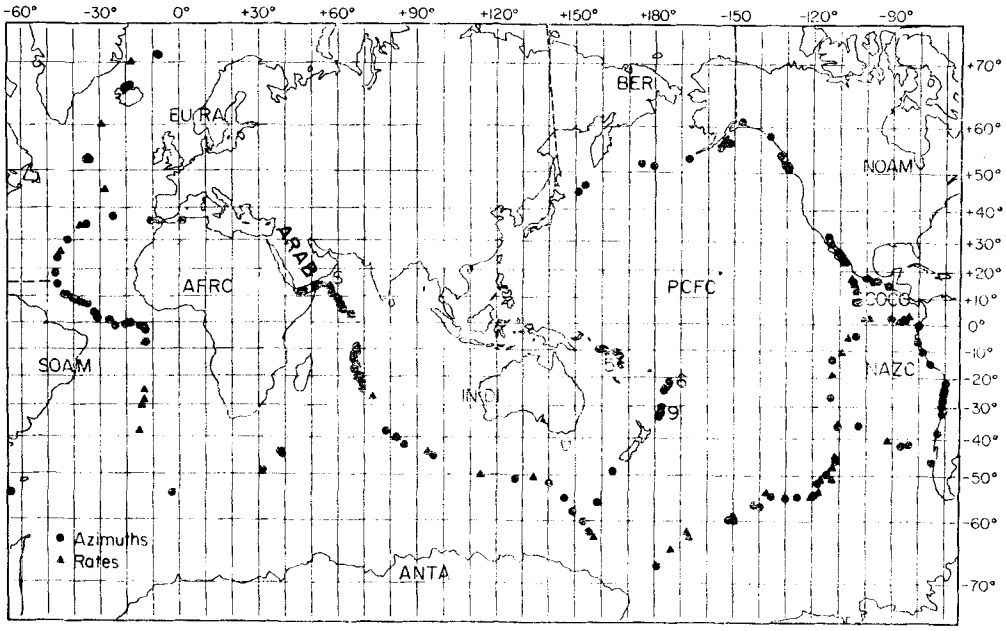

FIG. 1. Plate names and geographical distribution of the data used to compute model RM1. Numbers indicate the number of data with very close locations.

ranean region or in Asia (McKenzie 1972; Molnar, Fitch, T. J. & Wu, F. T., 1973b). In other regions, small plates clearly exist, but the data on their boundaries are inadequate to improve our knowledge about the major plates. Such complications create no problem provided that we include only data from well-defined plate boundaries and ignore data on irrelevant or doubtful boundaries. Therefore we have not included data from most of Asia or Indonesia.

Ten major plates are considered (Fig. 1). These include the six plates of Le Pichon (1968), but the Cocos and Nazca plates are detached from Antarctica, North and South America are separated from one another, and Arabia is separated from the Indian plate. The existence of resolvable motion between North and South America is an important result. As we shall see, the data also suggest the existence of an eleventh plate, the Bering plate.

After a brief presentation of the solution to the forward problem, we develop the inversion technique, and proceed with a presentation of the data set, the model, and the agreement between them. We next analyse the distribution of information along the plate boundaries. Finally, we test the Wilson–Morgan hypothesis and discuss its major physical implications.

2. Instantaneous plate kinematics

By a well-known theorem due to Euler, the instantaneous motion of a rigid plate constrained to lie on the surface of a sphere can be completely and uniquely described by an axial rotation. Therefore, the velocity field of a mosaic of m plates is determined by specifying the m instantaneous angular velocity vectors of these plates, referenced to some fixed frame with an origin at the centre of the sphere. With respect to this reference frame, the instantaneous velocity of a point $\mathbf{r}$ belonging to a plate P_i is

$$\mathbf{v}(\mathbf{r}) = \boldsymbol{\Omega}_i \times \mathbf{r}, \tag{1}$$

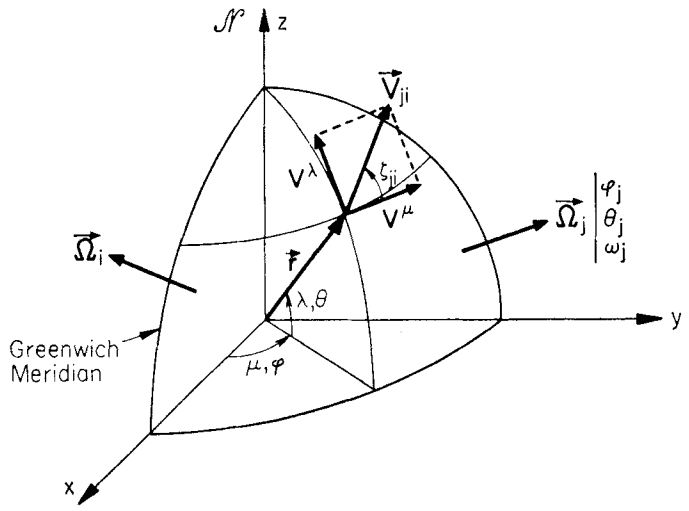

FIG. 2. Geometry of the instantaneous kinematic problem.

where $\mathbf{\Omega}_i$ is the angular velocity vector of P_i. If the point $\mathbf{r}$ is on the boundary of two plates P_i and P_j, then the relative velocity of P_j with respect to P_i at $\mathbf{r}$ is given by

$$\mathbf{v}_{ji}(r) = (\mathbf{\Omega}_j - \mathbf{\Omega}_i) \times \mathbf{r}. \tag{2}$$

Obviously, $\mathbf{v}_{ji} = -\mathbf{v}_{ij}$.

Any position vector $\mathbf{r}$ on the surface of the sphere is expressible in terms of the spherical co-ordinates (a, λ, μ), where a is the radius of the sphere, and λ and μ are the geographical co-ordinates latitude (positive north) and longitude (positive east). If θ_i and ϕ_i are the latitude and longitude of the rotation pole for the i-th plate, then the angular velocity vector $\mathbf{\Omega}_i$ for this plate has components $(\omega_i, \theta_i, \phi_i)$, where ω_i is the rate of rotation, taken to be positive in a right-handed sense. Since a relative velocity vector $\mathbf{v}_{ji}(\mathbf{r})$ is always tangent to the sphere, it can be expressed in terms of its latitudinal component $v_{ji}{}^\lambda$ and its longitudinal component $v_{ji}{}^\mu$. From equation (2) the following expressions can be derived:

$$\left.\begin{aligned} v_{ji}{}^\lambda &= a\omega_j \cos\theta_j \sin(\mu-\phi_j) - a\omega_i \cos\theta_i \sin(\mu-\phi_i). \\ v_{ji}{}^\mu &= a\omega_j(\cos\lambda \sin\theta_j - \sin\lambda \cos\theta_j \cos(\mu-\phi_j)) \\ &\quad - a\omega_i(\cos\lambda \sin\theta_i - \sin\lambda \cos\theta_i \cos(\mu-\phi_i)). \end{aligned}\right\} \tag{3}$$

These equations represent a solution to the *forward* problem: given the $3m$ parameters ω_i, θ_i, ϕ_i; $i = 1, \ldots, m$; we can compute the components of relative velocity between two plates at any point on their common boundary. The geometry described above is shown on Fig. 2, the details of the algebra leading to equation (3) are found in Appendix A.

3. The inverse problem of instantaneous plate kinematics

We are now in a position to examine the *inverse* problem of instantaneous plate kinematics: given some observations of the components of relative velocities at plate boundaries, what is the best representation of instantaneous motions?

Typically the independently observable quantities are the magnitudes v_{ji} and the

directions ζ_{ji} of relative motion defined by

$$\left.\begin{aligned} v_{ji} &= \|\mathbf{v}_{ji}\| = \sqrt{[(v_{ji}{}^{\lambda})^2 + (v_{ji}{}^{\mu})^2]}, \\ \zeta_{ji} &= \arctan\left[\frac{v_{ji}{}^{\lambda}}{v_{ji}{}^{\mu}}\right]. \end{aligned}\right\} \tag{4}$$

Using equations (3), explicit expressions for v_{ji} and ζ_{ji} in terms of the model parameters can be obtained.

Suppose there exist n_v estimates of the magnitudes of relative motion at the points $\mathbf{r}_1, \mathbf{r}_2 \ldots \mathbf{r}_{n_v}$, and n_ζ estimates of the direction of relative motion at the points $\mathbf{r}_{n_v+1}, \mathbf{r}_{n_v+2} \ldots \mathbf{r}_{n_v+n_\zeta}$. Then these values are the components of a vector $\mathbf{d}^0$ of length $N = n_v + n_\zeta$. In a similar fashion, the $3m-3$ independent components of a plate motion model can be juxtaposed to form a model vector $\mathbf{m}$:

$$\mathbf{m} = (\theta_1, \ldots, \theta_{n-1}, \phi_1, \ldots, \phi_{m-1}, \omega_1, \ldots, \omega_{m-1}), \tag{5}$$

where we have arbitrarily chosen the reference frame so that the m-th plate is fixed. For a relative motion model only $M = 3m-3$ components are independent. We define $\mathfrak{M}$ to be the vector space of all such models.

Equations (3) and (4) relate the data to the model; for any $\mathbf{m}$ we can compute the vector $\mathbf{d}(\mathbf{m})$. If the data were error free and perfectly compatible, the representation we seek would satisfy the equation

$$\mathbf{d}(\mathbf{m}) = \mathbf{d}^0. \tag{6}$$

However the observations are not perfectly compatible and are contaminated with errors. Let us assume that we deal with statistically independent observations and that they are free of bias. Rate data are obtained by measuring a distance between two anomalies along a magnetic profile, and we take the fundamental distribution for this process to be Gaussian. On the other hand, azimuth data will obey the statistics of directions. The fundamental distribution of errors on a unit circle (Von Mises distribution) or sphere (Fisherian distribution) has a density proportional to

$$\exp(\kappa \cos \beta),$$

where β is the angular error and κ is a measure of the dispersion (Fisher 1953). This distribution plays the same role in circular or spherical geometry as the Gaussian distribution plays in Euclidean geometry.

To obtain a model representation, one might maximize a likelihood function proportional to

$$\exp\left\{-\sum_{i=1}^{n_v} \frac{[d_i{}^0 - d_i(\mathbf{m})]^2}{2\sigma_i{}^2}\right\} \exp\left\{+\sum_{i=n_v+1}^{N} \kappa_i \cos[d_i{}^0 - d_i(\mathbf{m})]\right\},$$

where $d_i{}^0$ is the i-th component of $\mathbf{d}^0$, $d_i(\mathbf{m})$ is the value of the i-th data functional evaluated at $\mathbf{m}$, $\sigma_i{}^2$ $(i = 1, \ldots, n_v)$ the variance of the i-th rate datum, and κ_i $(i = n_v+1 \ldots N)$ the invariance of the i-th direction. A necessary and sufficient condition for the likelihood to be maximized is that the function

$$F = \sum_{i=1}^{n_v} \frac{[d_i{}^0 - d_i(\mathbf{m})]^2}{2\sigma_i{}^2} - \sum_{i=n_v+1}^{N} \kappa_i \cos[d_i{}^0 - d_i(\mathbf{m})] \tag{7}$$

be minimized. The function defined in equation (7) is a logical fitting function to use in the plate tectonic inverse problem. McKenzie & Sclater (1971) have suggested other fitting functions, but these do not take advantage of the fact that some data may be known better than others. In the function F, the data are weighted according to their uncertainties. This is a desirable property: rates having a large variance

σ_i^2, or directions having a small invariance κ_i, will play a less important role than the more accurate data. A quantitative evaluation of the effects of weighting will be discussed more extensively in Section 6.

F achieves a stationary value when its derivatives with respect to the model parameters are zero; that is, when

$$\sum_{i=1}^{n_v} \frac{(d_i^0 - d_i(\mathbf{m}))}{\sigma_i^2} \frac{\partial d_i(\mathbf{m})}{\partial m_j} + \sum_{i=n_v+1}^{N} \kappa_i \sin [d_i^0 - d_i(\mathbf{m})] \frac{\partial d_i(\mathbf{m})}{\partial m_j} = 0, \quad j = 1, \ldots, M. \quad (8)$$

Unfortunately, these equations are non-linear and cannot be readily solved for $\mathbf{m}$. In fact, a solution may not exist, and, if it does, we cannot show that it is unique.

These difficulties can be circumvented if the dispersions are small. For small dispersions ($\kappa_i \gg 1$) the Fisher and Von Mises distributions are well approximated by Gaussian distributions. Expanding the cosine function in a power series and truncating beyond the second term, we obtain

$$\exp \{\kappa_i \cos [d_i^0 - d_i(\mathbf{m})]\} \simeq \exp (\kappa_i) \exp \left\{ -\frac{\kappa_i}{2} [d_i^0 - d_i(\mathbf{m})]^2 \right\},$$

which is proportional to a Gaussian distribution with variance σ_i^2 if we set

$$\kappa_i = \frac{1}{\sigma_i^2}. \quad (9)$$

Since the power series expansion of $\cos(x)$ is alternating, an upper bound to the truncation error is given by the value of the first term of the remainder series, which is $[d_i^0 - d_i(\mathbf{m})]^4/4!$, provided that the terms in the series form a decreasing sequence tending to zero. The RMS value of $d_i^0 - d_i(\mathbf{m})$ is given by σ_i, and a large value of σ_i for the data we used is 20° or 0·35 radians. Thus the sequence is decreasing, and the approximation is valid when $\sigma_i^2/2! \gg \sigma_i^4/4!$ or when $\sigma_i^2/12 \ll 1$. Since for a 20° dispersion $\sigma_i^2/12 \simeq 0{\cdot}009$, the Gaussian approximation is quite justified.

Under a Gaussian approximation, equation (8) reduces to

$$\sum_{i=1}^{N} \frac{d_i(\mathbf{m})}{\sigma_i^2} \frac{\partial d_i(\mathbf{m})}{\partial m_j} = \sum_{i=1}^{N} \frac{d_i^0}{\sigma_i^2} \frac{\partial d_i(\mathbf{m})}{\partial m_j}, \quad j = 1, \ldots, M. \quad (10)$$

This equation is still non-linear in $\mathbf{m}$. However, if we can construct a reasonably good 'starting model' $\mathbf{m}^*$, these equations can be linearized. By good, we mean a model $\mathbf{m}^*$ for which the difference $\mathbf{m} - \mathbf{m}^*$ is small enough that $\partial d_i(\mathbf{m})/\partial m_j$ can adequately be approximated by $\partial d_i(\mathbf{m}^*)/\partial m_j$ for all i and j. In this case we can write

$$\sum_{k=1}^{M} \frac{\partial d_i(\mathbf{m}^*)}{\partial m_k} (m_k - m_k^*) = d_i(\mathbf{m}) - d_i(\mathbf{m}^*), \quad (11)$$

neglecting terms of order $(m_j - m_j^*)^2$. Now we subtract the quantity

$$\sum_{i=1}^{N} \frac{d_i(\mathbf{m}^*)}{\sigma_i^2} \frac{\partial d_i(\mathbf{m}^*)}{\partial m_j}$$

from both sides of (10). Evaluating all derivatives at $\mathbf{m}^*$ and applying equation (11), we obtain

$$\sum_{i=1}^{N} \sum_{k=1}^{M} \frac{1}{\sigma_i^2} \frac{\partial d_i}{\partial m_j} \frac{\partial d_i}{\partial m_k} (m_k - m_k^*) = \sum_{i=1}^{N} \frac{1}{\sigma_i^2} \frac{\partial d_i}{\partial m_j} [d_i^0 - d_i(\mathbf{m}^*)], \quad j = 1, \ldots, M. \quad (12)$$

Equation (12) is then a linear equation for the difference between the model we seek and the starting model $\mathbf{m}^*$.

We now define the following vectors and matrices

$$\delta\mathbf{m} = \mathbf{m} - \mathbf{m}^*; \quad \delta\mathbf{d}^0 = \mathbf{d}^0 - \mathbf{d}(\mathbf{m}^*); \quad A_{ik} = \frac{\partial d_i}{\partial m_k};$$

$$A_{ik}{}^T = A_{ki}; \quad V_{ik} = \sigma_i{}^2 \delta_{ik}.$$

The elements of $\mathbf{A}$ are given in Appendix B.

With these definitions equation (12) becomes, in operator notation,

$$\mathbf{A}^T \mathbf{V}^{-1} \mathbf{A} \delta\mathbf{m} = \mathbf{A}^T \mathbf{V}^{-1} \delta\mathbf{d}^0. \tag{13}$$

As long as there are as many independent data as model parameters, this equation has the unique solution

$$\delta\mathbf{m} = (\mathbf{A}^T \mathbf{V}^{-1} \mathbf{A})^{-1} \mathbf{A}^T \mathbf{V}^{-1} \delta\mathbf{d}^0,$$

the standard weighted least squares solution. The matrix $\mathbf{V}$ is the error auto-correlation matrix of the data and (in general) does not have to be diagonal, as we have assumed. The matrix $\mathbf{W} = (\mathbf{A}^T \mathbf{V}^{-1} \mathbf{A})^{-1}$ is easily shown to be the auto-correlation matrix of the errors in the solution induced by errors in the data (Matthews & Walker 1965).

The new estimate of the model is given by $\mathbf{m}^* + \delta\mathbf{m}$. This perturbation procedure is iterated until convergence is attained.

The matrix $\mathbf{W}$ is positive definite and defines on the model space $\mathfrak{M}$ a hyper-ellipsoid of uncertainty. By extracting from $\mathbf{W}$ the appropriate 3×3 matrices, symmetric with respect to the diagonal, one can define ellipsoids of uncertainty for each $\boldsymbol{\Omega}_i$, $i = 1, \ldots, m-1$. By extracting a 2×2 matrix corresponding to the latitude and longitude of a given pole, one similarly defines an ellipse of uncertainty in the tangent plane to the surface of the Earth at this pole. Doubling the principal axes of this ellipse will give a symmetric 95 per cent confidence region for this pole. Formally, the distributions corresponding to the extracted uncertainty matrices are marginal distributions of the multivariate normal distribution defined by $\mathbf{W}$.

The use of confidence regions is a convenient tool for the determination of whether two models are resolvable. Consider two determinations of a pole Π, Π_1 and Π_2, obtained from two different data sets. We shall say that Π_1 is resolvable from Π_2 at the 95 per cent confidence level, if it lies outside the 95 per cent confidence region of Π_2. It does not follow that Π_2 in turn is resolvable from Π_1. Indeed the data from which Π_2 was obtained may well carry enough information to forbid Π_1, while the data leading to Π_1 may have large enough uncertainties to make Π_2 a permissible solution.

The analysis can obviously be carried to any number of dimensions. A purist would argue that only entire model vectors can be compared. In practice one is rarely interested in comparing more than one pair of rotation vectors at a time.

4. The data set

To construct the data set we gathered as many relative motion data as we could, and then isolated from this collection those which we found to be most reliable (Table 1, Fig. 1). Most of the data are taken from the published literature, and discussion of each datum is unnecessary. However, a discussion of the possible errors and their evaluation is essential. Two uncertainties were independently assigned to each datum. One was based mainly on the quality of the measurement and did not require the existence of a model. The other assumed the form of the law of error to be Gaussian, and that a model could be fit to the data. The variances

Table 1

Data set used to compute model RM1. For rates, data, standard deviations, predicted values from model RM1, and residuals are in centimetres per year, for azimuths they are in degrees. Standard deviations are discussed in Section 4, importances are described in Section 6. The reference numbers correspond to those listed in the bibliography.

	LAT.N	LONG.E	DATA	S.D.	RM1	RESID.	IMP.	REF.
			****	PCFC	NOAM	****		
RATES	23.0	-108.5	5.6	0.4	5.7	-0.1	0.642	(58,59)
AZIM.	58.3	-136.9	N22W	10.	N21W	1.	0.093	(94)
	54.1	-132.6	N26W	10.	N23W	3.	0.088	(41)
	51.8	-131.0	N32W	10.	N25W	7.	0.084	(81)
	50.8	-130.0	N15W	15.	N26W	-11.	0.037	(107)
	31.7	-114.4	N51W	10.	N43W	8.	0.072	(101)
	29.7	-113.7	N45W	10.	N45W	0.	0.070	(101)
	29.3	-113.6	N48W	10.	N45W	3.	0.070	(90)
	26.7	-111.1	N53W	10.	N48W	5.	0.071	(90)
	26.3	-110.2	N49W	10.	N48W	1.	0.073	(101)
	25.3	-109.2	N45W	10.	N50W	-5.	0.074	(71)
	25.1	-109.8	N55W	10.	N49W	6.	0.072	(90)
	24.1	-109.0	N55W	10.	N50W	5.	0.073	(90)
	23.1	-107.9	N55W	10.	N52W	3.	0.074	(71)
			****	COCO	PCFC	****		
RATES	17.0	-105.7	9.4	0.4	9.3	0.1	0.279	(92)
	15.0	-104.5	9.6	0.4	10.0	-0.4	0.245	(92)
	13.0	-104.0	10.7	0.4	10.7	0.0	0.240	(92)
	12.5	-103.5	11.0	0.4	10.9	0.1	0.245	(37)
AZIM.	16.0	-105.0	N80E	10.	N85E	5.	0.113	(60)
	8.5	-104.0	N80E	10.	N84E	4.	0.070	(60)
	8.5	-103.0	N76E	15.	N83E	7.	0.029	(74)
			****	COCO	NOAM	****		
AZIM.	17.3	-100.1	N44E	15.	N39E	-5.	0.051	(74)
	16.3	-95.8	N36E	10.	N37E	1.	0.082	(74)
	16.0	-97.9	N40E	10.	N39E	-1.	0.096	(74)
	14.5	-91.7	N35E	10.	N37E	2.	0.062	(74)
			****	COCO	NAZC	****		
RATES	2.0	-101.0	4.5	1.0	4.8	-0.3	0.170	(40)
	2.0	-100.7	4.6	1.0	4.9	-0.3	0.163	(40)
	2.0	-100.2	5.0	1.0	4.9	0.1	0.153	(40)
	2.0	-99.6	5.0	1.0	5.0	0.0	0.141	(40)
	2.0	-98.7	5.8	1.0	5.1	0.7	0.124	(40)
	0.8	-87.5	6.4	0.4*	6.3	0.1	0.288	(39)
	0.8	-87.0	6.4	0.4*	6.4	0.0	0.296	(87)
	3.2	-83.9	6.4	0.4*	6.7	-0.3	0.407	(30)
AZIM.	2.0	-90.5	N 1W	10.	N 6W	-5.	0.322	(24)
	2.0	-85.5	N 0E	10.	N 6W	-6.	0.277	(114)
	1.5	-85.3	N 0E	20.	N 5W	-5.	0.069	(74)

	LAT.N	LONG.E	DATA	S.D.	RM1	RESID.	IMP.	REF.
			****	NAZC	PCFC	****		
RATES	-6.0	-106.5	16.4	1.0	16.6	-0.2	0.176	(89)
	-11.0	-108.0	16.8	1.0	17.2	-0.4	0.154	(89)
	-19.0	-113.0	18.0	1.0	17.9	0.1	0.141	(37)
AZIM.	-4.5	-104.0	S76E	10.	S79E	-3.	0.039	(1)
	-13.5	-113.0	S75E	20.	S75E	0.	0.010	(1)
	-26.9	-113.6	S84E	10.	S75E	9.	0.035	(100)
			****	NAZC	ANTA	****		
RATES	-40.5	-92.0	7.6	0.5	7.3	0.3	0.789	(54)
AZIM.	-36.0	-103.0	S82E	12.*	S79E	3.	0.112	(7)
	-36.2	-110.9	N82E	11.*	S73E	25.	0.138	(24)
	-41.7	-84.0	N86E	11.*	N85E	-1.	0.078	(24)
	-42.0	-87.0	S88E	11.*	N88E	-4.	0.080	(7)
			****	ANTA	SOAM	****		
AZIM.	-54.3	-63.6	N81E	10.	N79E	-2.	0.263	(81)
			****	PCFC	ANTA	****		
RATES	-35.6	-110.9	10.9	0.6	11.0	-0.1	0.087	(37)
	-45.0	-112.0	9.8	0.4	10.3	-0.5	0.117	(86)
	-48.0	-113.0	10.0	0.4	10.0	0.0	0.112	(86)
	-51.0	-113.0	10.0	0.4	9.7	0.3	0.110	(86)
	-51.2	-117.5	10.0	0.4*	9.6	0.4	0.108	(72)
	-54.0	-118.0	9.4	0.4	9.3	0.1	0.106	(72)
	-54.0	-138.0	9.0	0.6	8.8	0.2	0.045	(72)
	-55.0	-121.0	8.9	0.5	9.1	-0.2	0.066	(72)
	-59.0	-150.0	8.0	0.5	7.8	0.2	0.071	(86)
	-59.0	-151.0	7.4	0.5	7.7	-0.3	0.072	(72)
	-60.0	-150.0	7.8	0.5	7.7	0.1	0.073	(86)
	-62.0	-168.0	7.3	0.5	6.6	0.7	0.089	(72)
	-63.0	-167.0	6.2	0.5	6.5	-0.3	0.090	(86)
	-65.0	-174.0	6.3	0.8	5.9	0.4	0.040	(86)
AZIM.	-46.0	-112.5	N77W	5.	N77W	-0.	0.041	(72)
	-50.0	-115.0	N76W	5.	N76W	0.	0.044	(72)
	-52.8	-118.0	N72W	3.	N74W	-2.	0.131	(72)
	-54.3	-119.5	N71W	3.	N73W	-2.	0.135	(72)
	-55.0	-126.0	N68W	3.*	N70W	-2.	0.132	(72)
	-55.0	-130.0	N70W	3.*	N69W	1.	0.131	(72)
	-56.5	-143.0	N65W	3.*	N63W	2.	0.133	(72)
	-59.5	-151.0	N62W	5.	N59W	3.	0.071	(72)
	-54.8	-136.0	N61W	10.	N67W	-6.	0.013	(72)
	-56.6	-142.5	N61W	10.	N64W	-3.	0.015	(72)
	-67.5	-179.3	N51W	15.	N40W	11.	0.017	(72)

	LAT.N	LONG.E	DATA	S.D.	RM1	RESID.	IMP.	REF.
			****	NAZC	SOAM	****		
AZIM.	-0.7	-80.2	N78E	12.*	N81E	3.	0.045	(43)
	-6.9	-80.5	N74E	11.*	N82E	8.	0.044	(43)
	-10.7	-78.8	N72E	11.*	N81E	9.	0.045	(43)
	-14.9	-75.9	N88E	10.*	N80E	-8.	0.046	(43)
	-21.8	-70.0	N77E	10.	N77E	-0.	0.049	(43)
	-24.1	-70.3	N79E	10.	N77E	-2.	0.048	(43)
	-27.8	-71.1	N69E	10.	N78E	9.	0.045	(43)
	-25.5	-70.7	S84E	10.	N77E	-19.	0.046	(43)
	-27.9	-71.1	N75E	10.	N78E	3.	0.045	(43)
	-29.9	-71.4	N65E	10.	N78E	13.	0.044	(43)
	-30.0	-71.5	N87E	10.	N78E	-9.	0.044	(43)
	-31.4	-71.0	S87E	10.	N78E	-15.	0.044	(43)
	-31.9	-71.5	S86E	10.	N78E	-16.	0.043	(43)
	-38.1	-73.0	N79E	10.	N79E	-0.	0.042	(43)
	-46.4	-75.4	S87E	10.	N80E	-13.	0.043	(43)
			****	PCFC	INDI	****		
AZIM.	-9.7	158.7	S78W	15.	S78W	-0.	0.008	(50)
	-9.9	160.7	S56W	10.*	S79W	23.	0.018	(50)
	-10.6	161.4	S88W	11.*	S79W	-9.	0.018	(50)
	-10.9	165.3	S68W	20.	S82W	14.	0.005	(50)
	-12.3	166.4	S78W	20.	S82W	4.	0.005	(50)
	-14.9	166.9	S83W	20.	S82W	-1.	0.006	(50)
	-15.4	166.9	S60W	12.*	S82W	22.	0.018	(50)
	-15.6	167.3	S70W	12.*	S82W	12.	0.018	(50)
	-15.7	167.1	S58W	12.*	S82W	24.	0.018	(50)
	-15.8	167.5	S73W	12.*	S83W	10.	0.018	(50)
	-15.9	167.5	S70W	12.*	S83W	13.	0.018	(50)
	-21.8	-174.8	N70W	13.*	N84W	-14.	0.016	(44)
	-22.4	-174.9	N57W	13.*	N84W	-27.	0.016	(50)
	-22.8	-175.3	N74W	20.	N84W	-10.	0.007	(50)
	-23.3	-175.6	N72W	15.	N85W	-13.	0.013	(44)
	-23.6	-176.0	N72W	14.*	N85W	-13.	0.016	(44)
	-24.7	-176.7	N88W	14.*	N85W	3.	0.016	(44)
	-29.8	-177.2	N67W	16.*	N85W	-18.	0.016	(44)
	-29.9	-177.8	N76W	20.	N86W	-10.	0.011	(44)
	-29.9	-177.7	N85W	20.	N86W	-1.	0.011	(44)
	-30.1	-177.2	N74W	17.*	N85W	-11.	0.016	(44)
	-30.2	-177.8	N88W	20.	N86W	2.	0.011	(44)
	-30.5	-178.1	N84W	20.	N86W	-2.	0.011	(50)
	-30.7	-178.3	N76W	17.*	N86W	-10.	0.016	(50)
	-30.7	-178.3	N78W	17.*	N86W	-8.	0.016	(50)
	-30.9	-177.6	N90W	20.	N85W	5.	0.012	(50)
	-32.2	-178.1	N90W	20.	N86W	4.	0.013	(50)
	-33.5	-179.0	S72W	20.	N87W	21.	0.014	(50)
	-49.0	163.7	S56W	37.*	S58W	2.	0.016	(6)
	-56.2	158.2	S 0E	48.*	S27W	27.	0.014	(6)

	LAT.N	LONG.E	DATA	S.D.	RM1	RESID.	IMP.	REF.
			****	INDI	ANTA	****		
RATES	-27.0	73.0	6.0	0.4	6.1	-0.1	0.230	(70)
	-40.0	82.0	7.0	0.4	7.0	0.0	0.177	(70)
	-44.0	94.0	7.0	0.4	7.3	-0.3	0.156	(70)
	-50.0	114.0	7.5	0.4	7.5	0.0	0.170	(116)
	-50.5	134.0	7.4	0.4	7.2	0.2	0.222	(116)
	-63.0	157.0	6.8	0.4	6.8	0.0	0.281	(20)
AZIM.	-38.0	78.0	N48E	15.	N38E	-10.	0.019	(70)
	-40.0	82.0	N39E	15.	N36E	-3.	0.018	(70)
	-42.0	85.0	N34E	15.	N34E	-0.	0.017	(70)
	-45.0	96.0	N29E	15.	N26E	-3.	0.016	(70)
	-45.2	96.1	N17E	10.	N26E	9.	0.037	(6)
	-51.0	127.0	N 0E	5.	N 3E	3.	0.149	(32)
	-52.0	140.0	N12W	15.	N 8W	4.	0.018	(7,70)
	-55.2	146.1	N22W	15.	N14W	8.	0.018	(6)
	-55.3	146.2	N13W	25.	N14W	-1.	0.006	(6)
	-58.0	149.0	N19W	10.	N18W	1.	0.039	(32)
	-60.0	153.0	N19W	5.*	N23W	-4.	0.144	(32)
	-62.0	155.0	N22W	15.	N25W	-3.	0.017	(7,70)
			****	INDI	AFRC	****		
RATES	9.0	60.0	2.4	0.4	2.0	0.4	0.154	(70)
	7.0	61.0	2.4	0.4	2.2	0.2	0.150	(70)
	5.0	62.0	2.7	0.4	2.4	0.3	0.145	(70)
	3.0	65.0	2.8	0.4	2.8	0.0	0.131	(70)
	-11.0	67.0	4.2	0.5	3.9	0.3	0.080	(22,70)
	-12.0	66.0	4.0	0.6	3.9	0.1	0.056	(22,70)
	-16.0	67.0	3.9	0.5	4.2	-0.3	0.084	(22,70)
	-21.0	68.5	4.2	0.5	4.7	-0.5	0.093	(22,70)
	-24.5	69.0	4.6	0.5	4.9	-0.3	0.102	(22,70)
AZIM.	11.0	57.5	N30E	8.*	N34E	4.	0.341	(64)
	-9.0	67.0	N52E	4.*	N52E	-0.	0.213	(22)
	-14.0	66.0	N55E	3.*	N57E	2.	0.206	(22)
	-16.0	66.5	N60E	5.	N58E	-2.	0.080	(22)
	-17.5	66.0	N63E	3.	N59E	-4.	0.209	(22)
	-20.0	67.0	N60E	10.	N59E	-1.	0.018	(22)
	-20.0	68.0	N63E	10.	N58E	-5.	0.017	(22)
	-22.5	69.0	N65E	15.	N58E	-7.	0.007	(22)
			****	AFRC	ANTA	****		
RATES	-44.2	38.8	2.0	0.3	1.6	0.4	0.541	(8)
AZIM.	-44.0	38.2	N11E	10.	N13E	2.	0.348	(8)
	-44.5	39.0	N20E	10.	N13E	-7.	0.342	(8)
	-48.8	31.5	N17E	20.	N24E	7.	0.108	(102)

	LAT.N	LONG.E	DATA	S.D.	RM1	RESID.	IMP.	REF.
			****	AFRC	NOAM	****		
RATES	34.5	-37.5	2.8	0.3	2.8	0.0	0.315	(85)
	26.0	-45.0	3.2	0.3	3.1	0.1	0.384	(85)
AZIM.	35.0	-35.0	S77E	5.	S79E	-2.	0.113	(25)
	30.0	-42.3	S81E	4.*	S79E	2.	0.269	(33)
	23.9	-46.0	S76E	15.	S80E	-4.	0.016	(100)
	23.9	-46.0	S84E	5.	S80E	4.	0.147	(26)
	18.5	-46.8	S85E	10.	S80E	5.	0.033	(33)
			****	AFRC	EURA	****		
AZIM.	37.5	-24.7	S82W	25.	N84W	14.	0.392	(67)
	37.5	-24.8	N84W	22.*	N85W	-1.	0.508	(6)
	36.2	-10.5	N10W	25.	N23W	-13.	0.206	(27)
	36.2	-7.6	N10W	25.	N18W	-8.	0.169	(67)
	36.2	-7.6	N39W	20.	N18W	21.	0.265	(6)
	36.2	1.5	N10W	25.	N 8W	2.	0.096	(67)
	36.0	-10.6	N10W	25.	N23W	-13.	0.214	(67)
			****	AFRC	SOAM	****		
RATES	-7.5	-13.0	3.6	0.4	3.8	-0.2	0.195	(112)
	-24.9	-13.0	4.5	0.4	4.1	0.4	0.153	(17)
	-28.3	-13.0	3.9	0.4	4.1	-0.2	0.152	(17)
	-30.5	-14.0	4.0	0.2	4.1	-0.1	0.455	(17)
	-38.2	-15.0	4.0	0.5	4.0	0.0	0.107	(17)
AZIM.	14.5	-46.0	S89E	10.	S83E	6.	0.062	(33)
	10.8	-42.3	S88E	4.*	S86E	2.	0.209	(33,34)
	10.8	-42.3	S89E	4.*	S86E	3.	0.209	(113)
	10.8	-43.3	N90E	10.	S86E	4.	0.043	(100)
	10.2	-40.9	S86E	5.	S87E	-2.	0.142	(33,34)
	9.4	-40.0	S88E	5.	S88E	-0.	0.130	(33,34)
	8.8	-38.7	S88E	10.	S89E	-1.	0.030	(33,34)
	7.6	-36.6	S89E	10.	N89E	-2.	0.026	(33,34)
	7.2	-34.3	S89E	10.	N88E	-3.	0.025	(33,34)
	4.0	-31.9	N88E	10.	N86E	-2.	0.023	(33,34)
	1.9	-30.6	N86E	10.	N86E	-1.	0.023	(33,34)
	1.1	-26.0	N86E	10.	N83E	-3.	0.028	(33,35)
	-0.1	-18.0	N77E	5.	N78E	1.	0.178	(33,35)
	-0.2	-18.7	N88E	10.	N78E	-10.	0.042	(100)
	-0.5	-19.9	N85E	10.	N79E	-6.	0.039	(100)
	-1.1	-24.0	N81E	10.	N82E	1.	0.029	(33,35)
	-1.3	-14.5	N75E	4.*	N76E	1.	0.401	(33,35)
	-1.9	-12.9	N82E	10.	N75E	-7.	0.056	(33,35)
	-2.9	-12.5	N73E	10.	N75E	2.	0.056	(33,35)
	-7.5	-12.3	N73E	10.	N76E	3.	0.049	(33)
	-54.3	-2.4	N77E	20.	N70E	-7.	0.010	(6)

	LAT.N	LONG.E	DATA	S.D.	RM1	RESID.	IMP.	REF.
			****	EURA	NOAM	****		
RATES	85.0	90.0	1.0	0.4	0.9	0.1	0.383	(88)
	70.0	-18.0	1.6	0.3	1.9	-0.3	0.317	(48)
	60.0	-29.0	2.4	0.2	2.3	0.1	0.282	(104)
	45.0	-28.0	2.8	0.3	2.7	0.1	0.203	(35)
AZIM.	80.2	-1.0	S52E	10.	S54E	-2.	0.072	(10)
	79.8	2.4	S43E	10.	S52E	-9.	0.070	(10)
	79.8	2.4	S47E	10.	S52E	-5.	0.070	(10)
	79.0	2.5	S52E	10.	S53E	-1.	0.067	(48)
	71.0	-8.0	S65E	5.*	S66E	-1.	0.168	(48)
	70.9	-7.6	S65E	10.	S66E	-1.	0.048	(101)
	66.7	-18.2	S65E	10.	S73E	-8.	0.033	(10)
	66.5	-20.0	S82E	10.	S74E	8.	0.033	(4)
	66.3	-19.8	S73E	10.	S74E	-1.	0.032	(100)
	52.9	-34.2	S73E	10.	S83E	-10.	0.025	(101)
	52.5	-35.5	S84E	4.*	S83E	1.	0.185	(46)
	52.5	-33.5	S85E	4.*	S82E	3.	0.173	(23)
			****	ARAB	AFRC	****		
RATES	14.8	54.8	2.1	0.2	2.1	0.0	0.094	(61)
	14.7	55.6	2.2	0.2	2.1	0.1	0.121	(61)
	14.6	56.0	2.3	0.2	2.2	0.1	0.138	(61)
	14.4	53.6	2.1	0.2	2.1	0.0	0.070	(61)
	14.3	56.5	2.2	0.2	2.2	0.0	0.165	(61)
	13.7	57.3	2.2	0.2	2.2	0.0	0.219	(61)
	13.4	50.7	2.0	0.1	2.0	-0.1	0.183	(61)
	13.2	50.9	2.0	0.1	2.0	0.0	0.186	(61)
	12.1	45.8	1.9	0.1	1.9	0.0	0.392	(61)
	12.0	45.6	1.9	0.1	1.9	0.0	0.404	(61)
AZIM.	14.0	51.7	N30E	15.	N30E	-0.	0.077	(101)
	13.5	51.5	N30E	5.	N30E	0.	0.697	(61)
	12.0	46.0	N35E	10.	N34E	-1.	0.254	(61)
			****	PCFC	BERI	****		
AZIM.	61.0	-147.5	N24W	11.*	N11W	13.	0.360	(97)
	56.6	-152.2	N27W	10.	N26W	1.	0.255	(97)
	56.6	-152.9	N29W	10.	N26W	3.	0.230	(97)
	56.5	-154.4	N25W	10.	N26W	-1.	0.191	(97)
	55.7	-155.8	N24W	10.	N28W	-5.	0.199	(97)
	53.1	-167.6	N31W	10.	N35W	-4.	0.081	(96)
	51.4	179.1	N39W	10.	N40W	-1.	0.083	(95)
	51.9	174.6	N27W	10.	N41W	-14.	0.132	(95)
	46.5	153.2	N52W	10.	N51W	1.	0.238	(98)
	44.7	150.7	N49W	10.	N52W	-3.	0.230	(98)

were then estimated from the scatter in the data. In all cases we retained the largest of the two estimates of the error to construct the operator V. The Gaussian assumption was checked by a statistical test.

Truncating the data set

In constructing the data set, the first step was to eliminate possible data that may not pertain to the plates we are studying. For instance we did not use spreading rate data on the East Pacific Rise between the Rivera and Tamayo fracture zones, or the strike of the Rivera fracture zone (Larson 1972; Larson, Menard & Smith 1968), because of the likely presence of a Rivera plate (Atwater 1970; Molnar 1973). Because of the deformation in the Basin and Range province, we did not use data from the San Andreas system. Because of the possible presence of a small plate east of the Panama fracture zone (Molnar & Sykes 1969), we did not use this fracture zone to determine the relative motion between the Cocos and Nazca plates. Similarly, because of the spreading behind the north end of the Tonga arc and the southern portion of the New Hebrides arc (Chase 1971; Karig 1970; Karig & Mammerickx 1972), we rejected data from this region to obtain Pacific–India motion.

Relative velocities

Because geodetic measurements and integrated seismicity methods are not yet accurate enough to use here, all of the relative velocity data were obtained from spreading rates at ocean ridges determined from magnetic anomalies. We always examined the raw data, and the rates in Table 1 are our own determinations from the raw data. Whenever it was possible, the rate was measured symmetrically with respect to the ridge crest, from anomaly three to anomaly three, in the Pitman, Herron & Heirtzler (1968) numbering system. This anomaly was chosen because it is easily identified, is old enough to resolve the rate, but is not so old that changes in the rate will introduce significant errors. For some ridges such as at the mouth of the Gulf of California, north of the Tamayo Fracture Zone or at the Western end of the Cocos–Nazca boundary data do not extend as far as anomaly three. In these cases we used whatever was available, but assigned a large uncertainty because of the lack of resolution. On some slow spreading ridges, such as in the Indian Ocean, anomaly five was the first well-developed anomaly, and we used it to obtain a rate. The Talwani, Windisch & Langseth (1971) time scale was used in all cases. When using anomaly three, rates are about 7 per cent faster than when the Vine (1966) or Heirtzler *et al.* (1968) time scales are used. Because of this, the rates in Table 1 differ in many cases from the published values. All of the time scales are the same for anomaly five.

We were cautious about using some lines in which the anomalies were not well developed. For this reason, we used only one of Herron's (1972) profiles across the East Pacific Rise between the Pacific and Nazca plates and only one profile across for the Chile Ridge (Klitgord *et al.* 1973). In the latter case, the anomalies were more easily identified than in other published studies and yielded a different rate. In the North Atlantic, we used Pitman & Talwani's (1972) study as a guide. They had incorporated data of Philips (1967), Philips *et al.* (1969), Williams & McKenzie (1971), and Van Andel & Bowin (1968).

For all of the data we used, subjective uncertainties were assigned on the basis of agreement of the magnetic anomalies with the synthetic profiles, as well as on the resolution of the distance scale in published figures. When possible, original figures were used rather than published small reproductions. We did not compute synthetic profiles ourselves, however.

Several phenomena could introduce errors in these data, even when clear

anomalies are present. Changes in rates or errors in the Talwani *et al.* time scale would cause incorrect estimates of the instantaneous rate of motion. However, as all of the rates are averages over a few million years, such errors will probably not be important. Many rates are based on data from only one side of a ridge crest. Though apparently rare (Weissel & Hayes 1971), asymmetric spreading therefore could be a source of inaccuracy. In one region, the Chile Ridge, there is controversy over the strikes of both the fracture zones and the ridge crests (Forsyth 1972; Herron & Hayes 1969; Morgan, Vogt & Falls 1968). Klitgord *et al*'s (1973) profile runs obliquely to both, and as a result, the spreading rate is more uncertain than the raw data would suggest. Because of these possible problems, the assigned uncertainties were often larger than those that might be suggested by the scientists who did the original work.

Directions of relative motions

Two sources of data were used to obtain the directions of relative motion between plates: transform fault trends and the horizontal projections of slip vectors of earthquakes. Where detailed bathymetric studies have been made, such as in the North Atlantic, equatorial Atlantic, and north-east Indian Ocean, fracture zones are well defined. In most other regions detailed surveys have not been made, and trends of fracture zones are less certain. In a few cases such as south of Australia, earthquake epicentres are lineated well enough to be used to map fracture zones. In all of these cases, the assumption was made that these features are transform faults with pure strike-slip motion. In general there is no reason to doubt this assumption. In one case, however, we did not use the fault trends. Movement on the Fairweather Fault during the south-east Alaska earthquake in 1958 contained a significant dip-slip component. This dip-slip movement was detected in Stauder's (1960) fault plane solution of the earthquake, and his estimate of the slip vector differs by 18° from the strike measured in the field by Tocher (1960). Moreover, the slip vector for the 1972 July 30 Queen Charlotte Islands earthquake is consistent with that of the 1958 earthquake (R. Page, private communication). North of the Fairweather fault, fault plane solutions indicate primarily thrust faulting (Molnar, unpublished data). Because of this complexity we did not use the fault strikes from this region as Morgan (1968) did but relied entirely on the slip vectors of earthquakes.

We used only fault plane solutions for which the first arrival diagram was available and in all cases assigned an uncertainty in the slip vector of no less than 10°. Very rarely is even one nodal plane resolved to better than 5° to 10°. Moreover, lateral variations in Earth structure are likely to cause errors in the solutions that are difficult to evaluate quantitatively. Therefore, 10° seemed a reasonable lower bound. The most reliably determined solutions are for pure strike-slip motion on vertical fault planes. In these cases, knowledge of the depth of focus and of the velocity structure of the earth are not as important as in other cases. At island arcs, one nodal plane, the auxiliary plane, is usually very steeply dipping and the slip vector is quite well determined. The large lateral variations in velocity near island arcs, however, do add uncertainty to the measured slip vector (Toksöz, Minear & Julian 1971). The most poorly determined slip vectors are for earthquakes with nodal planes dipping at an angle close to 45°, and there is often ambiguity about which is the fault plane. Moreover, the determination of the nodal planes depends very much on the depth of focus assumed, the seismic velocity at the focus, and the upper mantle structure. For instance, three different solutions have been given for a large earthquake west of Gibraltar in 1969 (Fukao 1973; Lopez Arroyo & Udias 1972; McKenzie 1972). Fukao supplemented *P* wave first motions with surface wave amplitudes, and we used his result. Yet, if the depth of focus and *P*-wave velocity in the source region were in error (e.g. if the event occurred in the crust), his data would be fit with a solu-

tion quite different from the one he gave. Therefore, we assigned a large uncertainty to this datum (25°). Because of the ambiguity of the fault plane and because of the question of earth structure, we did not use earthquakes with normal faulting mechanisms at ocean ridges. In addition events that clearly reflected internal deformation of one plate were not used.

On the basis of the preceding discussion we isolated a set of 68 rates and 168 azimuths and assigned uncertainties to them. They are listed in Table 1, and Fig. 1 shows their geographical distribution. Note that most plates are reasonably well surrounded by data along their boundaries, which is obviously a desirable feature. Note also that no boundary is unduly weighted by a large number of data.

Most of the standard deviations listed in Table 1 are the subjective errors we assigned upon examination of each individual datum. However, in a few cases, the scatter in the data suggested uncertainties larger than our subjective estimates. For these data we calculated uncertainties using a procedure described below. These values are denoted in Table 1 by an asterisk.

Rate uncertainties, statistical approach

We assumed in Section 3 that the rate data had Gaussian errors. Let us make the further assumption that an estimator of the variance of the rotation rate for a given pole is

$$\sigma^2 = \langle(\omega_i - \bar{\omega})^2\rangle.$$

Here $\omega_i = R_i/a \sin A_i$ where A_i is the co-latitude of the i-th spreading rate R_i, measured from the pole of relative rotation, a is the radius of the Earth, and $\bar{\omega} = \langle\omega_i\rangle$. The averages are taken over the rate data pertaining to this particular pole. Considering a particular model for which $\omega = \omega^0$ and defining $\delta\omega_i = \omega^0 - \omega_i$ we write

$$\sigma^2 = \langle(\delta\omega_i - \delta\bar{\omega})^2\rangle,$$

and then the standard deviation of the i-th datum is

$$\sigma_i = \sigma a \sin A_i. \tag{15}$$

The geometrical significance of this relation is shown in Fig. 3(a). Equation (15) expresses that the *relative* uncertainty σ_i/R_i is a constant along a plate boundary. This result is not unreasonable as long as the anomalies can be identified clearly.

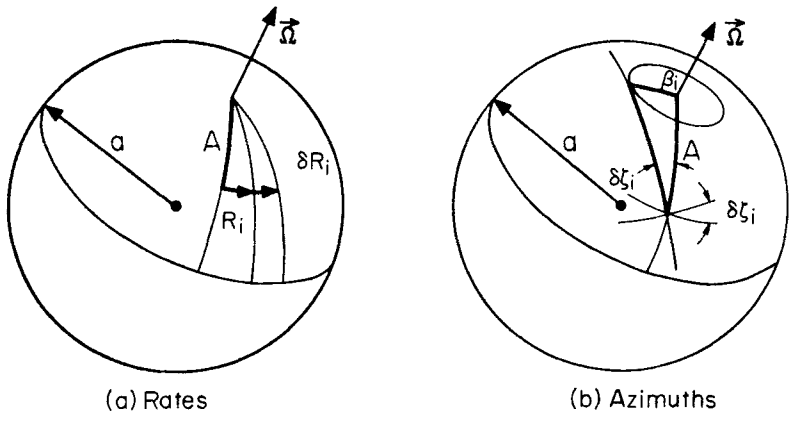

FIG. 3. Geometry for the statistical estimation of uncertainties in the data.

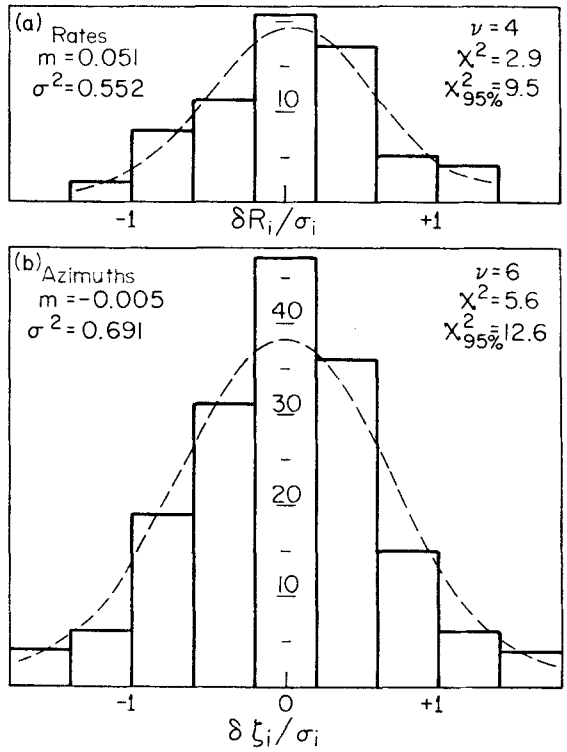

FIG. 4. Histograms of the normalized residuals distribution computed for model RM1. Dashed line represents theoretical Gaussian distribution. The results of the χ^2 test for normality at the 95 per cent confidence level are shown for reference. m = mean, σ^2 = variance, ν = degrees of freedom for χ^2 test.

If we have a good model, we expect $\overline{\delta\omega}$ to be close to zero, and the distribution of normalized residuals $\delta R_i/\sigma_i$ to be normal with variance one. Fig. 4(a) shows this distribution for all our rate data computed from our final model (described in Section 5). The normality of this distribution is successfully tested by a χ^2 test. The mean is close to zero, and the variance being smaller than one merely reflects the fact that we overestimated the standard deviations σ_i, by consistently choosing the larger of two estimates.

Azimuth uncertainties, statistical approach

We proceed for the azimuths in a very similar fashion. By definition, a pole of relative rotation between two plates is at the intersection of a family of great circles orthogonal to the direction of relative motion between these plates. However, if the datum ζ_i is contaminated by an error, $\delta\zeta_i$, the great circle perpendicular to this azimuth will pass within an angular distance $\beta_i = \arcsin(\sin\delta\zeta_i \sin A_i)$ from the pole. The geometry is described on Fig. 3(b). For unbiased data, we assume the β's have a Von Mises (Fisherian) distribution. However, we have shown earlier that for small errors the use of Gaussian statistics constitutes a valid approximation. The analysis is then carried out in the same way as for the rates. Thus defining for each pole

$$\sigma^2 = \langle \beta_i^2 \rangle,$$

where

$$\beta_i \simeq \delta\zeta_i \sin A_i,$$

and where the average is taken over the data pertaining to the particular pole under consideration, we get for the standard deviation of the i-th datum

$$\sigma_i = \sigma/\sin A_i, \tag{16}$$

which is the equivalent of (15) for azimuths. Under the assumptions stated above, data lying close to the equator of relative rotation will be fitted better than those lying in the vicinity of the pole. This is desirable since transform faults should be better developed and thus more easily mapped near the equator of relative rotation. Again, if we have a good model and the Gaussian approximation is correct, we expect the distribution of $\delta\zeta_i/\sigma_i$ to be normal, with a small mean and a variance of one. This distribution for all the azimuth data computed from our final model is shown in Fig. 4(b) and is tested successfully for normality. Again we have overestimated the errors in the data, for the computed variance is smaller than one.

In summary we have constructed a set of pertinent data to which we have assigned uncertainties. These uncertainties were chosen as the larger of two estimates. We can justifiably assume that these error processes are normal and are small enough to warrant use of a linear theory. In addition, by choosing a diagonal variance matrix **V**, we assume that the errors in the data are independent.

5. The model

Using the theory developed above we constructed a model of the instantaneous relative motions of eleven plates (Fig. 1): six large plates considered by Le Pichon (1968), but with North America and South America separated from one another and with the Cocos, Nazca, and Arabian plates. In addition we suggest the occurrence of internal deformation within the North American plate and model this by separating from North America the Bering plate, which includes the eastern end of Siberia, the Bering Sea, and the western part of Alaska.

Our final model, model Relative Motion 1 (RM1) was obtained in two successive steps: (1) construction of a starting model, and (2) iterative inversion of this starting model.

Because of the non-linearity of the problem, and because of the likely presence of local minima (Chase 1972; McKenzie & Sclater 1971), it was extremely important to construct an accurate starting model, $\mathbf{m}^*$. To do so, we first grouped the plates in triplets having a common triple junction, and inverted each triplet separately, using the pertinent data and starting with published angular velocity vectors. In no case were the poles thus obtained different from published ones by more than a few degrees, and in no case did they depend on the specific starting models. Because in general, the boundary between two plates has triple junctions at both ends, two different angular velocity vectors for the two plates could be obtained by inverting both triple junctions separately. In no case was there any large discrepancy between the two determinations. Thus consistency was checked from the very beginning. Having determined the 'best' angular velocity vector for each pair of plates, we then repeated the procedure using groups of four plates with two triple junctions. This 'accreting' process was performed until the last step where all the plates had to be considered simultaneously. By carefully monitoring the evolution of the different poles, and making sure that they undergo little change from one iteration to the next, we feel that we minimized the risk of slipping into a local minimum. That poles for the global model did not differ very much from those obtained from local studies provides *a posteriori* justification of this assertion.

For each inversion it was necessary to choose a reference frame, and an obvious choice of reference frame is to fix one of the plates. We found empirically that the procedure was less susceptible to instabilities if we fixed a plate with high relative velocity with respect to its neighbours and one with numerous neighbours, such as

Table 2

Model RM1. The first plate named moves counterclockwise with respect to the second one. Confidence intervals (C.I.) are obtained by doubling the standard deviation. They correspond to the intersection of the 95 per cent confidence ellipses by a parallel, meridian, and vertical line respectively.

Plate boundary	Lat. °N	C.I. deg.	Long. °E	C.I. deg.	Omega deg./My	C.I. deg./My
NOAM PCFC	50·9	3·4	−66·3	7·3	0·75	0·078
COCO PCFC	41·3	3·8	−108·1	4·2	2·02	0·261
COCO NOAM	31·8	3·6	−123·3	8·1	1·42	0·261
COCO NAZC	−2·9	8·4	−135·1	17·1	0·77	0·223
NAZC PCFC	56·6	5·9	−85·6	5·1	1·64	0·073
ANTA NAZC	−37·6	13·9	90·2	8·1	0·67	0·099
SOAM ANTA	−77·7	8·5	78·2	39·3	0·38	0·071
PCFC ANTA	−68·7	2·4	100·4	5·9	1·03	0·043
NAZC SOAM	51·9	10·4	−91·4	7·4	0·99	0·106
PCFC INDI	−59·8	2·1	178·0	4·2	1·26	0·068
INDI ANTA	10·7	4·7	31·6	3·6	0·67	0·029
INDI AFRC	18·7	3·5	44·8	2·9	0·58	0·052
INDI EURA	23·0	4·2	33·9	7·0	0·65	0·066
AFRC ANTA	−19·0	15·4	−13·3	18·1	0·19	0·045
AFRC NOAM	80·1	5·2	23·5	57·6	0·32	0·053
AFRC EURA	29·6	7·6	−25·7	5·6	0·14	0·085
AFRC SOAM	57·4	8·9	−37·5	4·7	0·37	0·028
NOAM SOAM	−3·0	20·1	−53·3	10·8	0·18	0·072
EURA NOAM	69·3	11·2	128·0	13·2	0·27	0·042
EURA PCFC	65·3	3·2	−69·8	10·1	0·91	0·088
INDI ARAB	7·4	6·1	65·5	6·5	0·39	0·160
ARAB AFRC	30·5	7·2	8·1	25·6	0·27	0·114
BERI PCFC	60·1	5·6	−114·4	47·2	—	—

the Pacific plate, rather than one moving slowly relative to its few neighbours, for instance Eurasia. We performed the inversion of the complete data set using the starting model described above, with the Pacific plate fixed in each iteration. Convergence was very rapid, and no significant improvement in the fit to the data was achieved after four iterations.

The observed data are compared with values calculated from the final model, RM1, in Table 1. The fit to the data set is clearly very good. That the entire data set can be explained by an eleven-plate model in itself is a strong argument in favour of the basic assumption that plates are rigid. Table 2 lists the pole positions and rotation rates and their uncertainties at the 95 per cent confidence level for model RM1. The pole positions and their uncertainty ellipses are depicted on Figs 5, 6 and 7. These 95 per cent confidence curves are ellipses if drawn in the plane tangent to the Earth's surface at the corresponding pole. Because of distortions introduced by the particular projection in each case, the curves shown in the figures are approximate, especially near the geographic poles where the geocentric co-ordinate system is singular. In addition, a selection of poles taken from the literature is shown for comparison.

The first important point to be noted is that model RM1 is not greatly different from previously published models. In particular, it closely resembles the global model of Morgan (1972a), and is reasonably close to Le Pichon's six-plate model (1968). Further, individual poles are often consistent with those obtained from local studies.

There are, however, a number of new features worth discussing.

North America was separated from South America and the separation was made—rather arbitrarily—along the 15° N parallel, where the distance between the mid-Atlantic ridge and the Lesser Antilles arc is the shortest. As a result, the AFRC–

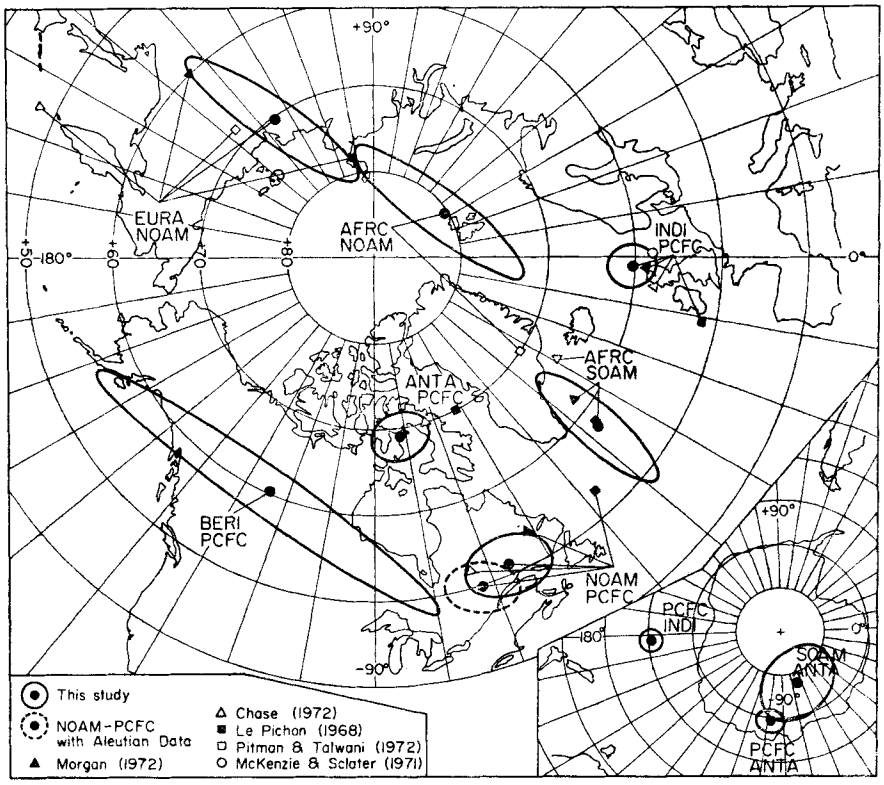

FIG. 5. Poles for model RM1 and other published poles. The 95 per cent confidence regions shown are ellipses drawn in the tangent plane to the surface of the Earth at the pole.

NOAM pole moved to the north-east, while the AFRC–SOAM pole remained in the vicinity of poles previously obtained from data along the mid-Atlantic ridge south of the Azores (Fig. 5). By the criteria defined in Section 3, these two poles are clearly resolvable from each other. One may wonder, however, whether this solution might represent a local minimum. To check this two independent inversions were performed, both treating North and South America as one single rigid plate. The first one used the AFRC–NOAM pole of RM1 as a starting pole between America and Africa, the second one used the AFRC–SOAM pole. In both cases the same pole between AFRC–AMER was obtained, in the vicinity of the one proposed by Pitman & Talwani (1972). We thus feel that a differential rotation between North and South America is resolvable. The NOAM–SOAM pole lies at the mouth of the Amazon River, and the rotation rate is about 0·2 deg/My (Fig. 6). This corresponds to a left lateral strike-slip component of motion along the 15° N parallel, with a rate of about 0·5 cm/yr. This is a slow rate, and the motion could be taken up by a slow inelastic deformation of the lithosphere. One can thus explain the low seismicity observed between North and South America.

Traditionally, the lithosphere north of the Aleutians arc has been considered part of the North American plate (McKenzie & Parker 1967). Under this assumption we determined a NOAM–PCFC pole at 49·5° N, 72° W, which agrees closely with Chase's (1972). But with this pole there is a systematic misfit to the slip vectors of earthquakes along the Aleutian and Kuril trenches. In addition, it is difficult to fit data on the AFRC–NOAM boundary. If one isolates data west of the 165° W meridian, and assigns them to a new plate (the Bering plate), one finds that they lead

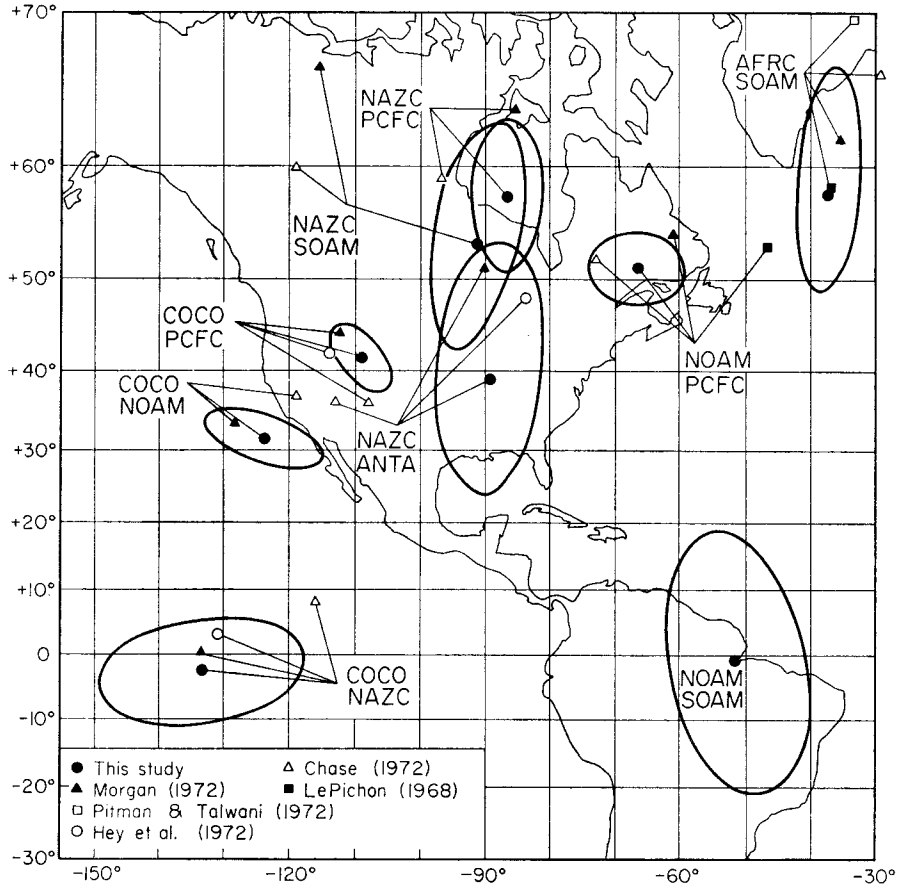

FIG. 6. See Fig. 5.

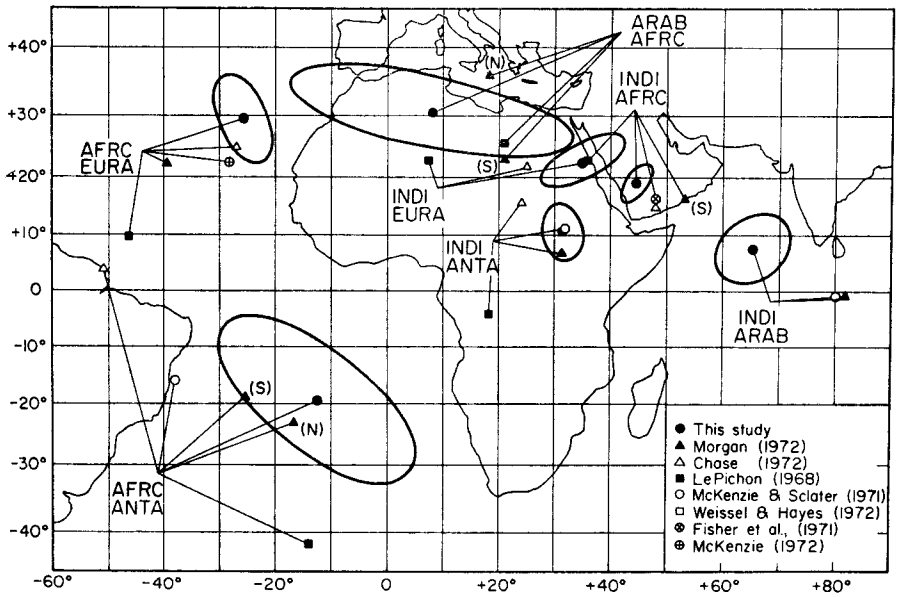

FIG. 7. See Fig. 5. Poles denoted by (S) pertain to the Somalian portion of Africa, those denoted by (N) to the Nubian portion.

to a quite different pole, denoted on Fig. 5 as BERI–PCFC. The NOAM–PCFC pole is now allowed to move eastward, giving better fits to data in the North-west Pacific, in the Gulf of California, and along the mid-Atlantic ridge. From Fig. 5 we see that the longitude of the BERI–PCFC pole is evidently poorly determined. However it seems to be resolvable from the NOAM–PCFC pole. On this basis we suggest the possible existence of a Bering plate, moving with respect to North America. At least, we may consider this as evidence of internal deformation of the North American plate. The broad zone of seismicity that extends into Alaska implies that deformation is occurring in this region. Unfortunately no reliable rate data are available along the PCFC–BERI or BERI–NOAM boundaries, and thus we cannot determine the relative angular velocity for either pair.

A similar problem is encountered in Africa (Fig. 7). There is evidence for a Somalian plate east of the East African rift zone (McKenzie *et al.* 1970). We did not succeed, however, in obtaining a satisfactory model in which Africa was separated into two plates. The reasons for this are that relative motion between Somalia and Africa is very slow and that estimates of the rates of opening are different by a factor of 2 or 3 (Baker, Mohr & Williams 1972; McKenzie *et al.* 1970; Searle 1970). Moreover, the rate and direction of opening in the Red Sea are poorly controlled by the data available. One can observe a trend in the misfit to the data along the Carlsberg ridge (the residuals change sign from north to south), which could possibly be corrected by separating Africa into a Nubian and a Somalian plate. However, all the data are fitted within their uncertainties, and this argument is by no means compelling.

Because of the complex deformation in Asia, only the data between Eurasia and North America and seven rather poorly determined slip vectors between Eurasia and Africa constrain the motion of the Eurasian plate with respect to other plates. The NOAM–EURA pole is at the mouth of the Lena River, but the 95 per cent confidence ellipse extends well south into Siberia (Fig. 5). Because there is geological evidence of a continental extension of the Arctic ridge into Siberia, the Moma Rift (Grachev, Demenitskaya & Karasik 1971), the pole may be in the southern portion of this ellipse. Refinements in the observed spreading rate in the Arctic will probably help reduce the uncertainty in this pole. Nevertheless, because the boundaries of the proposed Bering plate are not clear, we cannot eliminate the possibility that the spreading in the Arctic Ocean causes relative movement of the Eurasian and Bering, not North American, plates.

An important problem is to obtain a reliable estimate of the relative motion of the Pacific and North America plates, and then use this movement to examine the possible deformation in the Basin and Range province. There is only one datum for the rate of relative motion (Table 1), the Larson *et al.* (1968) rate for the opening of the Gulf of California. It is not well determined, but it is one of the most important data (Table 1). To remove some doubt about how much this datum might affect the results, we inverted all of the data, but without this rate and without the slip vectors in south-east Alaska and Western Canada. The data controlling the angular velocity of the Pacific and North America plates were the slip vectors and fault trends in the Gulf of California and the data from all of the other plates. Convergence was obtained rapidly giving essentially the same result as when all of the data are used. Thus, the relative motion of the Pacific and North American plates is well determined, and the rate of 5·6 cm/yr at the plate boundary is not likely to be in error by more than a few tenths of a centimetre per year.

The predicted rate of motion between the Pacific and North America in Central California is 5·5 cm/yr. From geodetic data Savage & Burford (1937) suggest a present rate of 3·2 cm/yr, along the San Andreas fault, and geologic evidence implies a similar rate for the last 10 My (Dickinson, Cowan & Schweickert 1972; Huffman

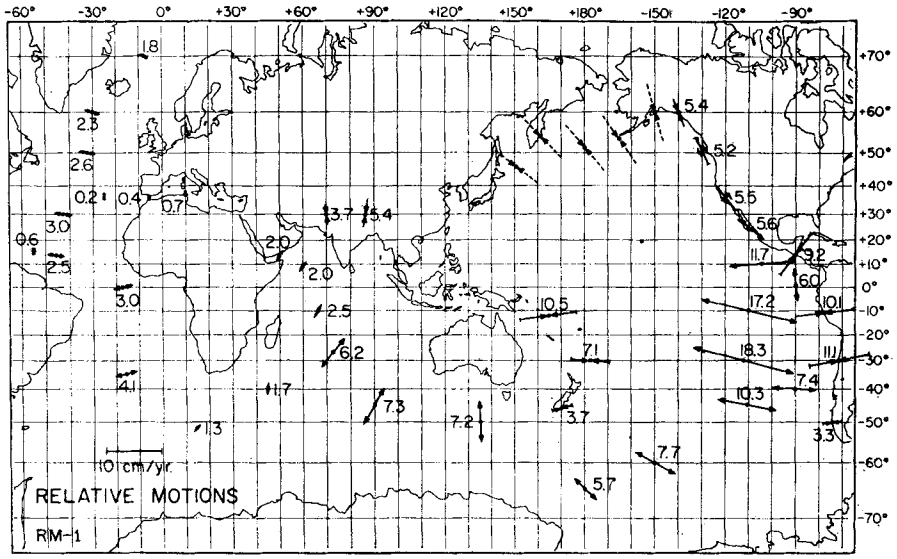

FIG. 8. Relative motions computed from model RM1 at selected points on plate boundaries. Numbers indicate total relative velocities in centimetres per year. Arrows indicate convergent, divergent, or transcurrent relative motion. Relative motions are drawn symmetrically for reasons of convenience only.

1972). The difference in the rates may be absorbed in the Basin and Range or along faults parallel to the San Andreas (Atwater 1970). On the other hand, the strike of the San Andreas north of the Transverse Ranges is indistinguishable from the direction of Pacific–North America motion (Fig. 8). This implies that extension in the Basin and Range is essentially parallel to the trend of the San Andreas fault.

6. Data importances and information distribution

We now analyse the information carried by the individual data in deriving model RM1. This is done in a fashion similar to that of Wiggins (1972), but we carry the analysis further, and make use of its predictive properties.

Since there are M unknowns, if the problem is overdetermined and to be solved in a least squares sense, we cannot have more than M linearly independent combinations of the data; their number should be exactly M if all the model parameters can be determined from the data set. Our present purpose is to show how one obtains these independent combinations and to investigate the partitioning of information among the different data.

Let us rewrite equation (13) in the form

$$\mathbf{A}^T \mathbf{V}^{-\frac{1}{2}} \delta\mathbf{D} = \mathbf{A}^T \mathbf{V}^{-\frac{1}{2}} \delta\mathbf{D}^0. \tag{17}$$

Here

$$\delta\mathbf{D} = \mathbf{V}^{-\frac{1}{2}}[\mathbf{d}(\mathbf{m}) - \mathbf{d}(\mathbf{m}^*)],$$

$$\delta\mathbf{D}^0 = \mathbf{V}^{-\frac{1}{2}}[\mathbf{d}^0 - \mathbf{d}(\mathbf{m}^*)].$$

The normalized perturbation vectors $\delta\mathbf{D}$ and $\delta\mathbf{D}^0$ (belonging to the Euclidian space $\mathbf{E}^N$) are dimensionless. This is convenient, especially because the data have different units.

Furthermore, we have, to first order,

$$\mathbf{V}^{-\frac{1}{2}} \mathbf{A} \delta\mathbf{m} = \delta\mathbf{D}. \tag{18}$$

From equation (18) $\delta\mathbf{D}$ lies in the range space of $\mathbf{V}^{-\frac{1}{2}}\mathbf{A}$, whereas this is not necessarily true for $\delta\mathbf{D}^0$. Let us solve (17) for $\delta\mathbf{D}$ as a function of $\delta\mathbf{D}^0$ using the pseudo-inverse solution (Penrose 1955; Jordan 1972). We get

$$\delta\mathbf{D}^0 = \mathbf{P}\delta\mathbf{D}^0, \tag{19}$$

where $\mathbf{P}$ is the symmetric operator

$$\mathbf{P} = \mathbf{V}^{-\frac{1}{2}}\mathbf{A}(\mathbf{A}^T\mathbf{V}^{-1}\mathbf{A})^{-1}\mathbf{A}^T\mathbf{V}^{-\frac{1}{2}}.$$

One may easily verify that $\mathbf{P}.\mathbf{P} = \mathbf{P}$, so that $\mathbf{P}$ is an orthogonal projection operator. If we diagonalize $\mathbf{P}$ the diagonal elements will be 0 or 1, and the rank of $\mathbf{P}$ will be the number of those elements which have value 1. In other words the rank of this operator is equal to its trace, tr $(\mathbf{P})$, which is an invariant. Equation (19) shows that each component of $\delta\mathbf{D}$ is a linear combination of those of $\delta\mathbf{D}^0$, and tr $(\mathbf{P})$ gives us the number of such independent combinations. Using the properties of orthogonal projection operators we write

$$\text{tr}\,(\mathbf{P}) = \sum_k P_{kk} = \sum_{ki}\sum P_{ik}{}^2 = \sum_k \frac{P_{kk}{}^2}{\sum_i P_{ik}{}^2}. \tag{20}$$

Clearly, P_{kk} is a measure of the relative contribution that the k-th component of $\delta\mathbf{D}$ receives from the k-th component of $\delta\mathbf{D}^0$. It is thus a measure of the independence of the k-th component of $\delta\mathbf{D}^0$ from the other components.

We define the importance $\mathscr{I}_k$ of the k-th datum by

$$\mathscr{I}_k = P_{kk}.$$

An importance $\mathscr{I}_k$ is a number such that $0 \leqslant \mathscr{I}_k \leqslant 1$, and the sum of all importances is the number of independent linear combinations of the data. If the problem is determinate, this sum equals M, the number of independent model parameters.

The main power of this definition lies in the fact that $\mathbf{P}$ does not depend on the actual values of the data and depends only weakly on the model $\mathbf{m}$. Thus the importance $\mathscr{I}_k$ of the k-th datum depends only on the nature and spatial distribution of the particular data set considered, and on the data uncertainties through the variance matrix $\mathbf{V}$. Also, importances are additive quantities: the importance of a subset of data is simply the sum of the importances of the individual data.

For example, let us consider the particular case of a data set consisting of N estimates of the same datum, with uncertainties $\sigma_1, \ldots, \sigma_N$, then the importance takes the form

$$\mathscr{I}_k = \frac{1}{\sigma_k{}^2\sum_i (1/\sigma_i{}^2)}.$$

As we can expect, $\sum_k \mathscr{I}_k = 1$ (from this data set we can determine only a 1-parameter model). If all the σ_i's are identical then

$$\mathscr{I}_i = \ldots = \mathscr{I}_N = \frac{1}{N},$$

which shows us qualitatively how the importance of one datum depends on its redundancy. On the other hand if

$$\sigma_1 = \sigma_2 = \ldots = \sigma_{N-1} \equiv \sigma$$

and

$$\sigma_N = \lambda\sigma \quad \lambda > 0,$$

then

$$\mathscr{I}_i = \ldots = \mathscr{I}_{N-1} = \frac{\lambda^2}{(N-1)\lambda^2+1}$$

and

$$\mathscr{I}_N = \frac{1}{(N-1)\lambda^2+1}.$$

These simple formulae show how the information is redistributed among the data when the variance of one datum is changed while everything else is fixed. If $\lambda > 1$, then $\mathscr{I}_N$ decreases, and accordingly the other data become more important. If $\lambda < 1$, the converse is true, and more information is carried by the N-th datum. For large N, the importance of a datum varies approximately as the inverse of its variance. These simple examples give us a qualitative idea of the the behaviour of $\mathscr{I}$.

In Table 1 are listed the importances of all the data. Their total sum is found to be 29·0, which is the number of model parameters we inverted for. The qualitative behaviour described above explains why the importances of azimuth data along the PCFC–INDI boundary are small: there is significant redundancy among these data. The effect of the size of the standard deviations σ_i can be seen on the set of azimuth data along the AFRC–SOAM or AFRC–NOAM boundaries: the less certain data are less important.

We tabulated the sums of the importances for the data on individual boundaries in Table 3. The distribution of information is as follows: 13·55 'independent data' for 68 magnitudes, and 15·45 for the 168 azimuths. As the Bering and Arabian plates are related each to only one other plate through the data, 2 and 3 independent data are associated respectively to the BERI–PCFC and ARAB–AFRC boundaries (the angular velocity of BERI–PCFC was not inverted for). Most ocean ridges are important plate boundaries, because all of the rate data and a large number of high quality azimuth data were gathered along them. Particularly noteworthy, however, is the AFRC–EURA boundary, which carries almost two 'independent data' distributed between only seven slip vector orientations of mediocre to poor quality.

Table 3

Information distribution

Boundary	Rates	Azimuths	Total
PCFC NOAM	0·642	0·953	1·595
COCO PCFC	1·010	0·212	1·222
COCO NOAM	0·0	0·291	0·291
COCO NAZC	1·743	0·668	2·411
NAZC PCFC	0·471	0·085	0·556
NAZC ANTA	0·789	0·408	1·197
ANTA SOAM	0·0	0·263	0·263
PCFC ANTA	1·188	0·865	2·053
NAZC SOAM	0·0	0·674	0·674
PCFC INDI	0·0	0·412	0·412
INDI ANTA	1·236	0·498	1·734
INDI AFRC	0·997	1·091	2·088
AFRC ANTA	0·541	0·799	1·340
AFRC NOAM	0·699	0·579	1·278
AFRC EURA	0·0	1·850	1·850
AFRC SOAM	1·063	1·810	2·873
EURA NOAM	1·185	0·976	2·161
ARAB AFRC	1·973	1·027	3·000
PCFC BERI	0·0	2·000	2·000
TOTALS	13·55	15·45	29·00

Apparently the geometry of the problem makes these data critical in determining the model. We do not have any rates of relative motion across this particular boundary. The predicted rate at the strait of Gibraltar by the model is 0·4 cm/yr. The fault plane solutions indicate a component of convergence and a component of transcurrent motion. If this rate could be measured to an accuracy of $\pm 0{\cdot}3$ cm/yr (i.e. ± 75 per cent of the predicted value), the importance of this datum, given our present data set, would be 0·24, and this would place it among the most important data of the set. We must emphasize here again that this last figure is independent of the (unknown) value of the rate, but depends on our model of plate geometry being correct.

The concept of data importances appears to be a powerful tool for the analysis of information distribution in a problem like this one. It permits us to single out plate boundaries where new data might prove particularly useful. If the data are ordered by decreasing importances we find that 50 per cent of the total information is provided by the 42 most important data, and 90 per cent by the 137 most important. As the total number of data is 236, this gives us a quantitative idea of the redundancy within the data set.

7. The hot spot hypothesis of Wilson and Morgan

Wilson (1963, 1965) proposed that plate motions over hotspots fixed in the mantle are responsible for the genesis of various island chains and aseismic ridges. The Hawaiian Islands in the Pacific and the Walvis Ridge in the South Atlantic are often quoted examples. Morgan (1971, 1972b) expanded Wilson's list of hotspots to include some twenty sites (each of which he associated with a mantle convection plume). Morgan (1972b) presented a model of plate motions over the mantle that is compatible with the directions of hotspot traces on the plates, supposing the hotspots to be fixed with respect to each other. We estimated the trends of 20 hotspot traces and using the Wilson–Morgan hypothesis and model RM1, systematically inverted these data to obtain a model of the instantaneous plate motions with respect to the hotspots. We view this procedure as a test of the Wilson–Morgan hypothesis: if a model can be found that satisfies the data to within its observational uncertainty, the Wilson–Morgan hypothesis, although not proved, cannot be rejected. Our results indicate that the available data are indeed consistent with this hypothesis.

If hotspots are fixed in some reference frame, which we assume to be in the mantle, the direction of a hotspot trace on a given plate away from the hotspot should equal the azimuth of the instantaneous motion of the plate in that frame. The directions of some traces, especially those on fast-moving plates such as the Pacific, are easily measurable to within ten degrees or so. On the other hand many traces, typically on the slow-moving plates, are represented by broad outpourings of lavas, and the actual direction of migration is quite uncertain. Masking by continental crust and transection by transform faults introduce additional sources of error in the interpretation of this kind of data. Observations are often further complicated by inadequate mapping or bathymetry. With due regard for these difficulties, we list in Table 4 our best estimates of the directions of the 20 hotspot traces, located on eight crustal plates, which we feel are measurable with an error less than several tens of degrees. The data used include 16 of the traces used by Morgan (1972), the Sierra Leone Ridge and the Martin Vaz chain in the Atlantic, the Kerguelen–Gaussberg Ridge in the Indian Ocean (Nougier 1970), and the trace of the Raton hotspot in New Mexico (Suppe & Powell 1973). Each measurement was assigned a subjective uncertainty of 10°, 20°, or 30°, depending on the quality of the observation (Table 4).

If we accept the hypothesis that hotspots form a rigid frame and that the relative motion model we have derived is essentially correct, then the motions of the plates

Table 4

Data for model AM1

Hotspot	Lat. (°N)	Long. (°E)	Trace	Plate	Obs. Az. (deg)	Comp. Az. (deg)	Res. (deg)	S.D.	Imp.	Rate (cm/yr)	Ref.
Hawaii	20	−155	Hawaiian Is. Chain	PCFC	N64W	N66W	−2·5	10	0·011	8·9	**(14)**
Juan de Fuca	46	−130	Cobb Seamounts	PCFC	N54W	N56W	−2·2	20	0·006	6·1	**(14)**
Easter	−27	−109	Tuamotu Chain	PCFC	N77W	N73W	+4·4	20	0·005	9·1	**(11)**
MacDonald	−29	−140	Austral Chain	PCFC	N65W	N66W	−0·6	10	0·017	8·5	**(49)**
Easter	−27	−109	Sala y Gomez Ridge	NAZC	N82E	S83E	+14·6	20	0·003	9·3	**(11)**
Galapagos	−1	−92	Carnegie Ridge	NAZC	S85E	N82E	−13·1	10	0·015	7·1	**(114)**
Galapagos	−1	−92	Cocos Ridge	COCO	N45E	N44E	−0·8	10	0·018	9·5	**(114)**
Kerguelen	−49	70	Kerguelen–Gaussberg Ridge	ANTA	S30E	S23E	+7·2	20	0·292	0·9	**(11)**
Prince Edward	−47	38	Prince Edward–Crozet	ANTA	N85E	N75E	+5·2	20	0·842	0·3	**(11)**
Reunion	−21	56	Reunion–Mauritius	AFRC	N45E	N38E	−7·3	10	0·542	1·7	**(22)**
Bouvet	−55	3	Bouvet–Meteor	AFRC	N30E	N42E	−11·6	10	0·311	2·0	**(47)**
Tristan da Cunha	−38	−11	Walvis Ridge	AFRC	N47E	N53E	+6·0	20	0·061	2·2	**(47)**
Ascension	−8	−14	Ascension	AFRC	N55E	N52E	−3·4	20	0·066	2·0	**(11)**
St Peter's and St Paul's Rocks	1	−29	Sierra Leone Ridge	AFRC	N52E	N57E	+4·5	30	0·037	1·7	**(11)**
Iceland	65	−17	Greenland–Iceland Ridge	NOAM	N43W	N46W	−2·5	20	0·140	2·3	**(11)**
Yellowstone	45	−110	Snake River Plain	NOAM	S60W	S72W	+11·7	20	0·038	2·7	**(106)**
Raton	37	−104	Raton	NOAM	S60W	S76W	+15·6	30	0·018	2·7	**(106)**
Tristan da Cunha	−37	−15	Rio Grande Ridge	SOAM	N73W	N80W	−5·0	30	0·042	2·2	**(11)**
Martin Vaz	−21	−29	Martin Vaz–Trinidad	SOAM	N88W	N74W	+13·9	10	0·45	2·3	**(11)**
Iceland	65	−17	Wyville–Thompson Ridge	EURA	S50E	N21E	−108·9	30	0·085	1·1	**(11)**

in that frame depend on only three independent parameters. The three parameters we chose to adjust are the three components of the Pacific angular velocity vector. (Of course, the rotation vector for any plate will do.) We applied the inversion procedure described in Section 3 to the azimuth data in Table 4. The inversion was initiated using Morgan's (1972) hotspot-Pacific pole (67° N, 73° W) and a rotation rate of 0·9°/My. Convergence was attained in six iterations, yielding a pole at 67·3° N, 59·4° W and an angular velocity of 0·83°/My. The angular velocity vectors for the eleven plates with respect to the hot spots constructed from this pole and from model RM1 are listed in Table 4 and shown in Fig. 9. This 'absolute' motion model is designated model AM1 (Table 5). The data functionals computed from model AM1, the data residuals, and the calculated importances are listed in Table 4.

The overall fit of this model to the data is quite good. All but one of the computed azimuths deviate from their measured values by less than 15°, a fit we consider acceptable given the uncertainties of measurement. The notable exception is the azimuth of the Iceland trace over the Eurasian plate. Here the computed value deviates from the observed direction of the Wyville–Thomson Ridge by over 100°. We shall return to this discrepancy below.

The distribution of information in this data set as indicated by the data importances deserves some discussion. Perhaps the most surprising result is the relative unimportance of the Pacific data (the Cobb, Hawaiian, Tuamotu, and Austral island chains). With a cumulative importance of 0·039, these data contain only 1·3 per cent of the information, despite their relatively small uncertainties. Small cumulative importances are also computed for the data associated with the Nazca and Cocos plates. Most of the information, about 95 per cent, comes from traces on the African, Antarctic, South American, and North American plates. The Antarctic plate with two measurable traces has a cumulative importance of 1·13. The five African traces have a cumulative importance of 1·03. Over 60 per cent of the information comes

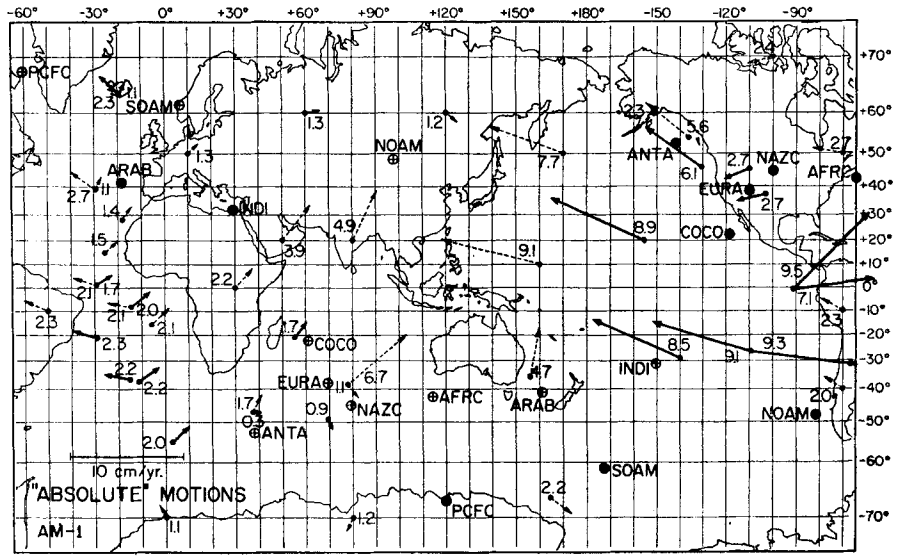

FIG. 9. Plate motions with respect to the hot spots computed from model AM1. Velocities are in centimetres per year. Poles and antipoles of plates in the hotspot frame are also shown. Heavy arrows indicate hot spots for which the trace was actually used in the inversion (Table 4). Dashed arrows represent velocity vectors computed at selected points.

Table 5

Model AM1. Plate rotation vectors in the hot spot reference frame. For convenience this frame in turn has been attached to the co-ordinate system shown in Fig. 2

Plate	Lat. °N	Long. °E	Omega deg/My
AFRC	42·2	−65·2	0·19
ANTA	52·7	−142·0	0·24
ARAB	41·2	−18·8	0·40
COCO	22·9	−118·7	1·47
EURA	38·1	−110·5	0·12
INDI	31·6	29·6	0·61
NAZC	44·7	−100·2	0·88
NOAM	−48·1	−82·1	0·24
PCFC	−67·3	120·6	0·83
SOAM	−61·7	−173·9	0·20

from three hotspot traces: the Prince Edward–Crozet trace on the Antarctic plate, the Reunion–Mauritius trace on the African plate, and the Martin Vaz trace on the South American plate. The Pacific hotspot rotation vector is thus mainly determined by traces observed on other plates. That this pole is close to those of Clague & Jarrard (1973), Morgan (1972) and Winterer (1973), which are based only on the trends of Island chains on the Pacific plate, is a strong argument in favour of the Wilson–Morgan hypothesis.

Following Morgan (1972), Duncan *et al.* (1972), and Burke *et al.* (1973) we took the Iceland hotspot trace on the Eurasian plate to be the Wyville–Thompson Ridge which has an azimuth of S 50° E. The importance of this datum is small, only 0·09, and the model is quite independent of its value. Nevertheless, the azimuth computed from model AM1 is N 21° E, yielding a residual of 109°. What is the cause of this discrepancy? One source of error is the relative motion model. However, the uncertainties in the relative motions are small enough to rule out this possibility.

Another possibility is that Iceland is moving with respect to the other hotspots. Combining the motion of the Eurasian plate predicted by model AM1 with a northward drift of the Icelandic hotspot of 1·3 cm/yr would yield a trace consistent with the Wyville–Thompson ridge. The trace on the North American plate would also be consistent with the Greenland–Iceland ridge. Thus, if the strike of Wyville–Thompson Ridge coincides with the direction of the Eurasian–Iceland motion during the last 10 My, then the Wilson–Morgan hypothesis must be accepted with qualification.

On the other hand, we do not consider the evidence for the motion of the Iceland hotspot particularly compelling. A simpler explanation is to admit that the Iceland trace on the Eurasian plate is not well delineated. Model AM1 is probably an adequate description of motions for only the last 10 My or so. The distance that the Eurasian plate has drifted over this hotspot during this time is only 110 km, less than the dimension of the island. It may be that the motion predicted by the model is approximately correct. The recent eruptions of Surtsey and Heimaey, south of Iceland, may in fact be evidence of northward motion of the Eurasian plate over the Iceland hotspot.

The rates of plate motion over the hotspots computed for model AM1 are listed in Table 4 and shown in Fig. 9. By dating rocks along the traces, it should be possible to determine these rates directly. Unfortunately, the volcanic activity at any particular site may persist for millions of years. Because of the practical difficulties in sampling and dating the oldest rocks along traces, this type of data has a tendency to be biased toward faster rates. For this reason we have excluded rate data from the actual inversion to obtain model AM1. It is interesting, however, to compare the predicted values with the data that do exist.

The most extensively studied trace is the Hawaiian–Emperor chain. A considerable literature exists, but the chronology of the chain is in dispute. Morgan (1972), using the potassium–argon dates of McDougall (1964) and Funkhouser, Barnes & Naughton (1968), gives a rate of 10·9 cm/yr averaged over the last 5 My and a rate of 5·5 cm/yr from 5 to 30 My. This second estimate is based on the early Miocene age assigned to Foraminifera found on Midway (Ladd, Tracey & Gross 1967, 1970). If this Midway date is correct, then the average rate over the last 30 My is 6·4 cm/yr.

More recently, Jackson, Silver & Dalrymple (1972) obtained an age of $16{\cdot}6 \pm 0{\cdot}9$ for Midway. Based on a least-squares fit to various radiometric age determinations (including their age of Midway), Jackson *et al.* obtained an average rate of 14·7 cm/yr, although they state that an average rate of 12·4 cm/yr cannot be ruled out. Our model AM1 predicts that the *present* rate of motion of the Pacific plate over the Hawaiian hotspot is 8·9 cm/yr. If the motion of the Pacific plate over the Hawaiian hotspot has been constant since Midway formed then either the hotspots are not fixed with respect to each other or Jackson *et al.*'s age for Midway is too young. Conversely if the hotspots are approximately fixed with respect to each other an age of 17 My for Midway requires that the Pacific plate has slowed since Midway formed.

Given that the Pacific is moving as a rigid plate over a set of relatively stationary hotspots, we have available a consistency check for the Hawaiian rates. Johnson & Malahoff (1971), using the potassium–argon age determinations of Krummenacher & Noetzlin (1966), give a rate of 9 cm/yr for the migration of volcanism along the Austral Chain. This may be compared with the model-predicted value of 8·5 cm/yr.

Haines (1973), using a statistical fit to the K–Ar data, has obtained rates ranging from 8·9 to 10·2 cm/yr at Hawaii and $7{\cdot}3 \pm 3{\cdot}4$ cm/yr for the Austral chain. In his analysis he deleted the datum for Midway.

McDougall & Chamalaun (1969) have summarized the geochronology of Reunion and Mauritius. The oldest lavas on Reunion seem to have an age of 2 My. On Mauritius the oldest volcanics date about 7·5 My, corresponding to an average rate of 2·9 cm/yr. The model predicts a somewhat smaller value of 1·7 cm/yr.

In a recent study, Armstrong, Leeman & Malde (1973) have dated a number of rocks on the Snake River Plain, the presumed trace of the Yellowstone hotspot. They have confirmed earlier determinations that indicated increasing in age to the south-west. Ages obtained for rhyolites in the Sublett Range, 250 km south-west of the Island Park Caldera, show a grouping near 10 My. This corresponds to a rate of 2·5 cm/yr, close to the model-predicted value of 2·7 cm/yr.

8. Discussion and conclusions

The theory of maximum likelihood has been adapted and applied to the inverse problem of instantaneous plate kinematics. Because a large number of data can be handled through this procedure, and because all the plates constituting the model can be considered simultaneously, this method is considerably more powerful than the more standard approaches. The remarkable fit to the data that we obtained is a convincing justification of the fundamental ideas of plate tectonics. A rigid plate model explains satisfactorily the features observed at plate boundaries on a global scale. Moreover, using a linear approximation, we can deduce the uncertainty in the model generated by the errors in the data. It has been shown that, provided that adequate precautions are taken, the non-linearity of the problem does not generate any major difficulties. The concept of data importances permits a particularly convenient display of the distribution of information within the data set.

Because the model is constrained to be self-consistent, systematic trends in the data become more apparent. Two examples were encountered in this study: The

presence of resolvable motion between North and South America, and the suggested existence of a Bering plate are important conclusions of this work. It can be expected that the accumulation of more numerous and better data will reduce the uncertainties in model RM1. We shall then possess a powerful tool to investigate internal plate deformations, as well as to model diffuse plate boundaries such as in Asia.

The same method was used to test the Wilson–Morgan hotspot hypothesis. Our conclusion is that the available trends of island chains can be fit within observational errors, if one assumes the hotspots fixed with respect to each other. Because the analysis does not make use of finite rotations this conclusion holds only for the last 10 My or so. It is highly surprising that trends of hot spot traces averaged over much longer periods of time can be fitted with an instantaneous model. This conclusion, which does not require any assumption about the nature and mechanism of hotspots, speaks strongly in favour of the Wilson–Morgan hypothesis. It becomes nevertheless increasingly urgent to verify the relative fixity of hotspots for much longer intervals; this check is beyond the power of the present study. Information about the rates of motion, as provided by rock dating will then become critical.

Within the restrictions presented above, model AM1 represents the plates motions in the hotspot frame. It exhibits several noteworthy features.

(1) Fig. 10 shows approximate average plate velocities with respect to the hotspots. In this frame oceanic plates move at an average rate of 10 cm/yr, about five times faster than continental plates. One may speculate that this is correlated with the presence of a better developed low velocity zone beneath oceans, oceanic plates undergoing thereby a lesser resistance to horizontal motion.

(2) At all subduction zones, the overthrusting plate has a small component of motion normal to the plate boundary, but may have a significant component of velocity parallel to the trench axis. Most of the relative motion is then taken up by a high subduction rate of the underthrusting plate. Moreover, it appears that trenches where the overthrusting plate has a lower velocity normal to the trench axis (e.g. the Kurile trench) give rise to a seismic zone dipping more steeply than in the converse case (e.g. the Chile Trench). Talwani (1969) argued that trenches have slow relative motions. Tullis (1972) also suggested that downgoing slabs act as anchors preventing rapid migration of the Trench axis, and tried to interpret the dips of seismic zones in this manner. Model AM1 seems to corroborate these suggestions.

(3) Using a computer program kindly provided by W. Kaula, we expanded the velocity field depicted on Fig. 9 in vector spherical harmonics. The coefficients of the toroidal harmonic of degree one gives the amount of net rotation of the lithosphere in the chosen frame. Model AM1 possesses a net westward rotation of 0·11°/My

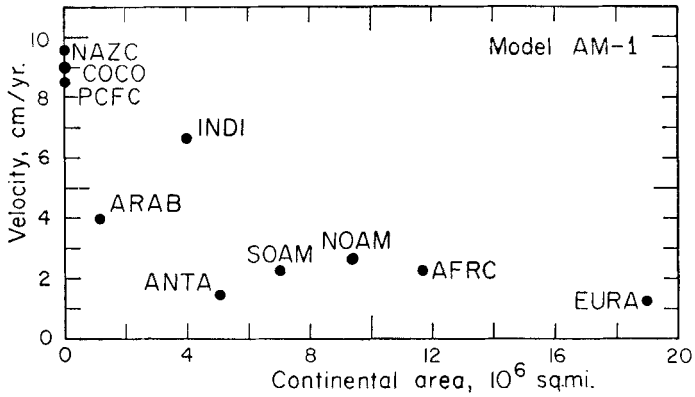

FIG. 10. Approximate average velocity of plates with respect to the hotspots, plotted against approximate continental area on each plate (above sea level).

around a pole situated at 129° E, 74° S. This is a very slow rotation; in fact, a model with no net rotation would fit acceptably well most of the traces in Table 4. The rate of motion of the Pacific plate at Hawaii would then be 7·8 cm/yr.

These last observations could provide useful boundary conditions for the dynamical models of plate tectonics. A more detailed discussion of these features, and a discussion of their implications are undertaken in another paper.

Acknowledgments

We are grateful to many scientists, too numerous to list, who gave us data in advance of publication.

This research was supported by JPL account code 49-615-95650-0-3910, National Science Foundation Grants NSF-GA-29755, NSF-GA-36804 and NASA contract NAS 7-100.

J. B. Minster:
Seismological Laboratory, California Institute of Technology, Pasadena, California 91109.

T. H. Jordan:
Princeton University, Department of Geological and Geophysical Sciences, Princeton, New Jersey.

P. L. Molnar:
Institute for Geophysics and Planetary Physics, University of California, San Diego, La Jolla, California.

E. Haines:
Division of Geological and Planetary Sciences, California Institute of Technology, Pasadena, California 91109.

References

(1) Andersen, R. N. & Sclater, J. G., 1972. Topography and evolution of the East Pacific Rise between 5 °S and 20 °S, *Earth Planet. Sci. Lett.*, **14,** 433–441.
(2) Armstrong, R. L., Leeman, W. P. & Malde, H. E., 1973. K–Ar Dating, Neogene volcanic rocks of the Snake River Plain, Idaho, in press.
(3) Atwater, T., 1970. Implications of plate tectonics for the Cenozoic tectonic evolution of western North America, *Bull. geol. Soc. Am.*, **81,** 3513–3536.
(4) Avery, O. E., Burton, G. D. & Heirtzler, J. R., 1968. An aeromagnetic survey of the Norwegian Sea, *J. geophys. Res.*, **73,** 4583.
(5) Baker, B. H., Mohr, P. A. & Williams, L. A. J., 1972. Geology of the eastern rift system of Africa, Special Paper 136, *Geol. Soc. Am.*
(6) Banghar, A. R. & Sykes, L. R., 1969. Focal mechanisms in the Indian Ocean and adjacent regions, *J. geophys. Res.*, **74,** 632.
(7) Barazangi, M. & Dorman, J., 1968. World seismicity map of ESSA Coast and Geodetic survey epicenters data for 1961–1967, *Bull. seism. Soc. Am.*, **59,** 369.
(8) Bergh, H., 1971. Sea floor spreading in the Southwest Indian Ocean, *J. geophys. Res.*, **76,** 5276.
(9) Burke, K., Kidd, F. S. W. & Wilson, J. T., 1973. Plumes and concentric plume traces of the Eurasian plate, *Nature Phys. Sci.*, **241,** 128.

(10) Conant, D. A., 1973. Six new focal mechanism solutions for the Arctic and a center of rotation for plate movements, *Bull. seism. Soc. Am.*, **63,** in press.
(11) *Chart of the world*, U.S. Navy Hydrographic Office, 1961, 10th edition.
(12) Chase, C. G., 1971. Tectonic history of the Fiji plateau, *Bull. geol. Soc. Am.*, **82,** 3087–3110.
(13) Chase, C. G., 1972. The *N*-plate problem of plate tectonics, *Geophys. J. R. astr. Soc.*, **29,** 117.
(14) Chase, T., Menard, H. W. & Mammerickx, J., 1971. *Bathymetry of the North Pacific*, Scripps Institute of Oceanography and Institute of Marine Resources, La Jolla, California.
(15) Clague, D. A. & Jarrard, R. D., 1973. Tertiary Pacific plate motion deduced from the Hawaiian emperor chain, *Bull. geol. Soc. Am.*, **84,** 1135–1154.
(16) Dickinson, W. R., Cowan, D. S. & Schweickert, R. A., 1972. Test of New Global Tectonics: Discussion, *B.A.A.P.G.*, **56,** 375.
(17) Dickson, G. O., Pitman, W. C. & Heirtzler, J. R., 1968. Magnetic anomalies in the South Atlantic Ocean and ocean floor spreading, *J. geophys. Res.*, **73,** 2087.
(18) Dietz, R. S. & Holden, J. C., 1970. Reconstruction of Pangea; Breakup and dispersion of continents, Permian to present, *J. geophys. Res.*, **75,** 4939.
(19) Duncan, R. A., Petersen, N. & Hargraves, R. B., 1972. Mantle plumes and the movement of the European plate, *Nature*, **239,** 82.
(20) Falconer, R. H. K., 1972. The Indian–Antarctic–Pacific triple junction, *Earth Planet. Sci. Lett.*, **17,** 151–158.
(21) Fisher, R. A., 1953. Dispersion on a sphere, *Proc. R. Soc. A*, **217,** 295.
(22) Fisher, R. L., Sclater, J. G. & McKenzie, D. P., 1971. The evolution of the central Indian ridge, Western Indian Ocean, *Bull. geol. Soc. Am.*, **82,** 553.
(23) Fleming, H. S., Cherkis, N. Z. & Heirtzler, J. R., 1970. The Gibbs fracture zone: a double fracture zone at 52° 30′ N in the Atlantic Ocean, *Mar. geophys. Res.*, **1,** 37.
(24) Forsyth, D. W., 1972. Mechanisms of earthquakes and plate motions in the East Pacific, *Earth Planet. Sci. Lett.*, **17,** 189.
(25) Fox, P. G., Lowrie, A. & Heezen, B. C., 1969. Oceanographer fracture zone, *Deep Sea Res.*, **16,** 59.
(26) Fox, P. J., Pitman, W. C. & Shephard, F., 1969. Crustal plates in the central Atlantic: evidence for at least two poles of rotation, *Science*, **165,** 487.
(27) Fukao, Y., 1973. Thrust faulting at a lithospheric plate boundary—the Portugal earthquake of 1969, *Earth Planet. Sci. Lett.*
(28) Funkhouser, J. G., Barnes, I. L. & Naughton, J. J., 1968. Determination of ages of Hawaiian volcanoes by K–Ar method, *Pacific Sci.*, **22,** 369–372.
(29) Grachev, A. F., Demenitskaya, R. M. & Karasik, A. M., 1971. *The Moma continental rift, and the problem of its structural relation with the mid-Atlantic ridge*, Abstract, Int. Union Geodesy and Geophysics, Moscow, Aug. 1971.
(30) Grim, P. J., 1970. Connection of the Panama fracture zone with the Galapagos rift zone, Eastern Tropical Pacific, *Mar. geophys. Res.*, **1,** 85.
(31) Haines, E. L., 1973. Modeling the movement of the Pacific plate with respect to the mantle, Abstract, *Trans. Am. geophys. Un.*, **56,** 472.
(32) Hayes, D. E. & Connolly, J. R., 1972. Morphology of the Southeast Indian Ocean, *Antarctic Oceanology II:* the *Australian–New Zealand Sector*, ed. Hayes, D. E., *Am. Geophys. Union*, Washington, D.C., 125.
(33) Heezen, B. C. & Tharp, M., 1965. Tectonic fabric of the Atlantic and Indian Oceans and continental drift, *Phil. Trans. R. Soc.*, **258.**
(34) Heezen, B. C., Gerard, R. D. & Tharp, M., 1964. The Vema fracture zone in the equatorial Atlantic, *J. geophys. Res.*, **69,** 733.

(35) Heezen, B. C., Bunce, E. T., Hersey, J. B. & Tharp, M., 1964. Chain and Romanche fracture zones, *Deep Sea Res.*, **11,** 11.

(36) Heirtzler, J. R., Dickson, G. O., Herron, E. M., Pitman, W. C. & Le Pichon, X., 1968. Marine magnetic anomalies, geomagnetic field reversals and motions of the sea floor and continents, *J. geophys. Res.*, **73,** 2119–2136.

(37) Herron, E. M., 1972. Sea-floor spreading and the Cenozoic history of the East-Central Pacific, *Bull. geol. Soc. Am.*, **83,** 1671.

(38) Herron, E. M. & Hayes, D. E., 1969. A geophysical study of the Chile ridge, *Earth Planet. Sci. Lett.*, **6,** 77–83.

(39) Herron, E. M. & Heirtzler, J. R., 1967. Sea-floor spreading near the Galapagos, *Science*, **158,** 775.

(40) Hey, R. N., Deffeyes, K. S., Johnson, G. L. & Lowrie, A., 1972. The Galapagos triple junction and plate motions in the East Pacific, *Nature*, **237,** 20.

(41) Hodgson, J. H. & Milne, W. G., 1951. Direction of faulting in certain earthquakes of the North Pacific, *Bull. seism. Soc. Am.*, **41,** 221.

(42) Huffman, O. F., 1972. Lateral displacement of upper Miocene rocks and the Neogene history of offset along the San Andreas fault in central California, *Bull. geol. Soc. Am.*, **83,** 2913–2946.

(43) Isacks, B. (in preparation).

(44) Isacks, B., Sykes, L. R. & Oliver, J., 1969. Focal mechanisms of deep and shallow earthquakes in the Tonga–Kermadec region and the tectonics of island arcs, *Bull. geol. Soc. Am.*, **80,** 1143.

(45) Jackson, E. D., Silver, E. A. & Dalrymple, G. B., 1972. The Hawaiian–Emperor chain and its relation to Cenozoic circumpacific tectonics, *Bull. geol. Soc. Am.*, **83,** 601–618.

(46) Johnson, G. L., 1967. North Atlantic fracture zones near 53°, *Earth Planet. Sci. Lett.*, **2,** 445.

(47) Johnson, G. L., Hey, R. N. & Lowrie, A., 1973. Marine geology in the environs of Bouvet Island and the South Atlantic triple junction, *Marine Geophys. Res.*, in press.

(48) Johnson, G. L., Southall, J. R., Young, P. W. & Vogt, P. R., 1972. Origin and structure of the Iceland plateau and Kobeinsey ridge, *J. geophys. Res.*, **77,** 5688.

(49) Johnson, R. M. & Malahoff, A., 1971. Relation of the MacDonald volcano to migration of volcanism along the Austral chain, *J. geophys. Res.*, **76,** 3282.

(50) Johnson, T. & Molnar, P., 1972. Focal mechanisms and plate tectonics of the Southwest Pacific, *J. geophys. Res.*, **77,** 5000.

(51) Jordan, T. H., 1972. *Estimation of the radial variation of seismic velocities and density in the Earth*, Ph.D. Thesis, California Institute of Technology.

(52) Karig, D. E., 1970. Ridges and basins of the Tonga–Kermadec Island arcs system, *J. geophys. Res.*, **75,** 239.

(53) Karig, D. E. & Mammerickx, J., 1972. Tectonic framework of the New Hebrides Island arc, *Marine Geol.*, **12,** 187.

(54) Klitgord, K. D., Mudie, J. D., Grow, J. & Larson, P. A., 1973. East sea-floor spreading on the Chile ridge, *Earth Planet. Sci. Lett.*, in press.

(55) Krummenacher, D. & Noetzlin, J., 1966. Ages isotopiques K/A de roches prelevees dans les possessions francaises du Pacifique, *Bull. Soc. Geol. de France*, **8,** 173–175.

(56) Ladd, H. S., Tracey, J. I. & Gross, M. G., 1967. Drilling on Midway Atoll, Hawaii, *Science*, **156,** 1088–1094.

(57) Ladd, H. S., Tracey, J. I. & Gross, M. G., 1970. Deep drilling on Midway Atoll, *U.S. Geol. Survey Prof. Paper* 680-*A*, A1–A22.

(58) Larson, R. L., 1972. Bathymetry, magnetic anomalies and plate tectonic history of the mouth of the Gulf of California, *Bull. geol. Soc. Am.*, **83,** 3345.

(59) Larson, R. L., Menard, H. W. & Smith, S. M., 1968. Gulf of California—a result of sea-floor spreading and transform faulting, *Science*, **161,** 781.

(60) Larson, R. L. & Chase, C. G., 1970. Relative velocity of the Pacific, North America and Cocos plates in the Middle America region, *Earth Planet. Sci. Lett.*, **7,** 425.

(61) Laughton, A. S., Whitmarsh, R. B. & Jones, M. T., 1970. The evolution of the Gulf of Aden, *Phil. Trans. R. Soc.*, **267,** 227.

(62) Le Pichon, X., 1968. Sea-floor spreading and continental drift, *J. geophys. Res.*, **73,** 3661.

(63) Lopez Arroyo, D. & Udias A., 1972. Aftershock sequence and focal parameters of the February 28, 1969 earthquake of the Azores–Gibraltar fracture zone, *Bull. seism. Soc. Am.*, **62,** 699.

(64) Matthews, D. H., 1966. The Owen fracture zone and the northern end of the Carlsberg ridge, *Phil. Trans. R. Soc.*, **259,** 172.

(65) Matthews, J. & Walker, R. L., 1965. *Mathematical methods of physics*, Benjamin, N.Y.

(66) McDougall, I. & Chamalaun, T. H., 1969. Isotopic dating and geomagnetic polarity studies on volcanic rocks from Mauritius, Indian Ocean, *Bull. geol. Soc. Am.*, **80,** 1419.

(66a) McDougall, I., 1964. Potassium–argon ages from lavas of the Hawaiian Islands, *Bull. geol. Soc. Am.*, **75,** 107–128.

(67) McKenzie, D., 1972. Active tectonics of the Mediterranean region, *Geophys. J. R. astr. Soc.*, **30,** 109.

(68) McKenzie, D. P., Davies, D. & Molnar, P., 1970. Plate tectonics of the Red Sea and East Africa, *Nature*, **226,** 243–248.

(69) McKenzie, D. P. & Parker, R. L., 1967. The North Pacific, an example of tectonics on a sphere, *Nature*, **216,** 1276–1280.

(70) McKenzie, D. P. & Sclater, J. G., 1971. The evolution of the Indian Ocean since the late Cretaceous, *Geophys. J. R. astr. Soc.*, **25,** 437.

(71) Molnar, P., 1973. Fault plane solutions of earthquakes and direction of motion in the Gulf of California and on the Rivera fracture zone, *Bull. geol. Soc. Am.*, **84,** in press.

(72) Molnar, P., Atwater, T. & Mammerickx-Winterer, J., 1973a. Magnetic anomalies, bathymetry and tectonic evolution of the South Pacific ocean floor since the late Cretaceous, (in preparation).

(73) Molnar, P., Fitch, T. J. & Wu, F. T., 1973b. Fault plane solutions of shallow earthquakes and contemporary tectonics in Asia, *Earth Planet. Sci. Lett.*, in press.

(74) Molnar, P. & Sykes, L. R., 1969. Tectonics of the Caribbean and Middle American regions from focal mechanism and seismicity, *Bull. geol. Soc. Am.*, **80,** 1639.

(75) Morgan, W. J., 1968. Rises, trenches, great faults and crustal blocks, *J. geophys. Res.*, **73,** 1959–1982.

(76) Morgan, W. J., 1971. Convection plume in the lower mantle, *Nature*, **230,** 42–43.

(77) Morgan, W. J., 1972a. Plate motions and deep mantle convection, *Geol. Soc. Am., Memoir* 132.

(78) Morgan, W. J., 1972b. Deep mantle convection plumes and plate motions, *Bull. Am. Assoc. Pet. Geol.*, **56,** 203–213.

(79) Morgan, W. J., Vogt, P. R. & Falls, D. E., 1968. Magnetic anomalies and sea-floor spreading on the Chile Rise, *Nature*, **222,** 137–142.

(80) Nouguier, J., 1970. Contribution a l'etude geologique et geomorphologique des iles Kerguelen, *Comite National Francais pour les recherches Antarctiques*, **27,** 696.

(81) Nyman, D., private communication.

(82) Penrose, R., 1955. A generalized inverse for matrices, *Proc. Camb. phil. Soc.*, **51,** 406.

(83) Philips, J. D., 1967. Magnetic anomalies over the Mid-Atlantic Ridge near 27° N, *Science*, **157,** 920–923.

(84) Philips, J. D., Thompson, G., Von Herzen, R. P. & Bowen, U. T., 1969. The Mid-Atlantic Ridge near 43° N latitude, *J. geophys. Res.*, **74,** 3069–3081.

(85) Pitman, W. C. & Talwani, M., 1972. Sea-floor spreading in the North Atlantic, *Bull. geol. Soc. Am.*, **83,** 619.

(86) Pitman, W. C., Herron, E. M. & Heirtzler, J. R., 1968. Magnetic anomalies in the Pacific and sea-floor spreading, *J. geophys. Res.*, **73,** 2069.

(87) Raff, A., 1968. Sea-floor spreading—another rift, *J. geophys. Res.*, **73,** 3699.

(88) Rassokho, A. I., Senchura, L. I., Deminitskaya, R. M., Karasik, A. M., Kicelev, Yu. G. & Trmoshenko, N. K., 1967. The mid-Arctic range as a unit of the Arctic Ocean mountain system, *Dokl. Akad. Nauk SSSR*, **172,** 659.

(89) Rea, D., Dymond, J., Heath, G. R., Heinrichs, D. F., Johnson, S. H. & Hussong, D. M., 1973. New estimates of rapid sea-floor spreading rates and the identification of young magnetic anomalies on the East Pacific Rise, 6° and 11° S, *Earth Planet. Sci. Lett.*, in press.

(90) Rusnack, G. A., Fisher, R. L. & Shephard, F. P., 1964. Bathymetry and faults of Gulf of California, *Marine Geology of the Gulf of California, Memoir* 3, of the *Am. Assoc. Pet. Geol.*, **59.**

(91) Savage, J. C. & Burford, R. O., 1973. Geodetic determination of relative plate motion in Central California, *J. geophys. Res.*, **78,** 832.

(92) Sclater, J. G., Anderson, R. N. & Bell, M. L., 1971. Elevation of ridges and evolution of the Central East Pacific, *J. geophys. Res.*, **76,** 788.

(93) Searle, R. C., 1970. Lateral extension in the East-African Rift Valleys, *Nature*, **227,** 267–268.

(94) Stauder, W., 1960. The Alaska earthquake of July 10, 1958: seismic studies, *Bull. seism. Soc. Am.*, **50,** 293.

(95) Stauder, W., 1968. Mechanism of the Rat Island earthquake sequence of February 4, 1965, with relation to island arcs and sea-floor spreading, *J. geophys. Res.*, **73,** 3847.

(96) Stauder, W., 1968. Tensional character of earthquake foci beneath the Aleutians, *J. geophys. Res.*, **73,** 7693.

(97) Stauder, W. & Bollinger, G. A., 1966. The focal mechanism of the Alaska earthquake and its aftershocks, *J. geophys. Res.*, **71,** 5283.

(98) Stauder, W. & Bollinger, G. A., 1966. The *S*-wave project for focal mechanism studies, earthquakes of 1963, *Bull. seism. Soc. Am.*, **56,** 1363.

(99) Suppe, J., Powell, C. and Berry, R., 1973. Regional Topography, Seismicity, Volcanism, and the present-day Tectonics of the Western United States, *Stanford Univ. Pubs. Geol. Sci.*, **13,** 181.

(100) Sykes, L. R., 1967. Mechanism of earthquakes and nature of faulting on the mid-ocean ridges, *J. geophys. Res.*, **72,** 2131.

(101) Sykes, L. R., 1970. Focal mechanism solutions for earthquakes along the world rift system, *Bull. seism. Soc. Am.*, **60,** 1749.

(102) Sykes, L. R., 1970. Seismicity of the Indian Ocean and a possible nascent island arc between Ceylon and Australia, *J. geophys. Res.*, **75,** 5041.

(103) Talwani, M., 1969. Plate tectonics and deep sea trenches, (abstract), *Trans. Am. geophys. Un.*, **50,** 180.

(104) Talwani, M., Windisch, C. C. & Langseth, M. G., 1971. Reykjanes ridge crest: a detailed geophysical study, *J. geophys. Res.*, **76,** 473.

(105) Tarling, D. H. & Gale, N. H., 1968. Isotope dating and paleomagnetic polarity in the Faeroe Islands, *Nature*, **218,** 1043.

(106) *Tectonic Map of North America*, U.S.G.S., 1969.

(107) Tobin, D. G. & Sykes, L. R., 1968. Seismicity and tectonics of the north-east Pacific Ocean, *J. geophys. Res.*, **73,** 3821.

(108) Tocher, D., 1960. Movement on the Fairweather fault and field investigation of the southern epicentral region, *Bull. seism. Soc. Am.*, **50,** 267.

(109) Toksöz, M. N., Minear, J. W. & Julian, B. R., 1971. Temperature field and geophysical effects of a downgoing slab, *J. geophys. Res.*, **76,** 1113.

(110) Tullis, T. E., 1972. Evidence that lithospheric slabs act as anchors (abstract), *Trans. Am. geophys. Un.*, **53,** 522.

(111) Van Andel, T. H. & Bowin, C. O., 1968. Mid-Atlantic Ridge between 22° and 23° north latitude, and tectonics of mid-ocean rises, *J. geophys. Res.*, **73,** 1279.

(112) Van Andel, T. H. & Moore, T. C., 1970. Magnetic anomalies and sea-floor spreading in the northern South Atlantic, *Nature*, **226,** 328.

(113) Van Andel, T. H. & Heath, G. R., 1970. Tectonics of the mid-Atlantic ridge, 6–8° south latitude, *Mar. geophys. Res.*, **1,** 5.

(114) Van Andel, T. H., Heath, G. R., Malfait, B. T., Heinrichs, D. F. & Ewing, J. I., 1971. Tectonics of the Panama Basin, eastern equatorial Pacific, *Bull. geol. Soc. Am.*, **82,** 1489.

(115) Vine, F. J., 1966. Spreading of the ocean floor; new evidence, *Science*, **154,** 1405–1415.

(116) Weissel, J. K. & Hayes, D. E., 1972. Magnetic anomalies in the south-east Indian Ocean, Antarctic Oceanology II: *the Australian–New Zealand Sector*, ed. D. E. Hayes, *Am. Geophys. Un.*, Washington, D.C., 165.

(117) Wiggins, R., 1972. The general linear inverse problem: Implication of surface waves and free oscillations for earth structure, *Rev. Geophys. Space Phys.*, **10,** 251.

(118) Williams, C. A. & McKenzie, D. P., 1971. The evolution of the north-east Atlantic, *Nature*, **232,** 168.

(119) Wilson, J. T., 1963. A possible origin of the Hawaiian Islands, *Can. J. Phys.*, **41,** 863–870.

(120) Wilson, J. T., 1965. Evidence from ocean island suggesting movement in the Earth, *R. Soc. Lond., Phil. Trans.*, **258,** 145–165.

(121) Winterer, E. L., 1973. Sedimentary facies and plate tectonics of equatorial Pacific, *Bull. Am. Assoc. Pet. Geol.*, **57,** 265.

Appendix A

Forward problem

From equation (2) we have

$$\mathbf{v}_{ji}(\mathbf{r}) = (\boldsymbol{\Omega}_j - \boldsymbol{\Omega}_i) \times \mathbf{r}.$$

From Fig. 2, the Cartesian components of these vectors are

$$\mathbf{r} \begin{vmatrix} a\cos\lambda\cos\mu \\ a\cos\lambda\sin\mu \\ a\sin\lambda \end{vmatrix} \qquad \boldsymbol{\Omega}_i \begin{vmatrix} \omega_i\cos\theta_i\cos\phi_i \\ \omega_i\cos\theta_i\sin\phi_i \\ \omega_i\sin\theta_i. \end{vmatrix}$$

The Cartesian components of $\mathbf{v}_{ji}$ are then

$$V_x = a\{\sin\lambda(\omega_j\cos\theta_j\sin\phi_j-\omega_i\cos\theta_i\sin\phi_i)-\cos\lambda\sin\mu(\omega_j\sin\theta_j-\omega_i\sin\phi_i)\}$$

$$V_y = a\{\cos\lambda\cos\mu(\omega_j\sin\theta_j-\omega_i\sin\theta_i)-\sin\lambda(\omega_j\cos\theta_j\cos\phi_j-\omega_i\cos\theta_i\cos\phi_i)\},$$

$$V_z = a\cos\lambda\{\omega_j\cos\theta_j\sin(\mu-\phi_j)-\omega_i\cos\theta_i\sin(\mu-\phi_i)\}.$$

We then obtain the longitudinal and latitudinal components $V_{ji}{}^{\mu}$ and $V_{ji}{}^{\lambda}$ by taking the inner product of $\mathbf{v}_{ji}$ with the unit tangents to the meridian and the parallel passing through $\mathbf{r}$. We get

$$V_{ji}{}^{\mu} = -\sin\lambda\cos\mu V_x-\sin\lambda\sin\mu V_y+\cos\lambda V_z,$$

$$V_{ji}{}^{\mu} = -\sin\mu V_x+\cos\mu V_y,$$

from which equations (3) are easily deduced.

Appendix B

Calculation of the matrix A

The elements of the matrix A are given by $A_{ik} = (\partial d_i/\partial m_k)$. From equation (4) we see that if d_i is of the form

$$d_i = V_{jl} = \sqrt{[(V_{jl}{}^{\lambda})^2+(V_{jl}{}^{\mu})^2]},$$

then

$$\frac{\partial V_{jl}}{\partial m_k} = \frac{V_{jl}{}^{\mu}}{V_{jl}}\frac{\partial V_{jl}{}^{\mu}}{\partial m_k}+\frac{V_{jl}{}^{\lambda}}{V_{jl}}\frac{\partial V_{jl}{}^{\lambda}}{\partial m_k}. \tag{B1}$$

On the other hand if d_i is of the form

$$d_i = \zeta_{jl} = \arctan\left[\frac{V_{jl}{}^{\lambda}}{V_{jl}{}^{\mu}}\right],$$

Then

$$\frac{\partial\zeta_{jl}}{\partial m_k} = \frac{V_{jl}{}^{\mu}}{V_{jl}{}^{2}}\frac{\partial V_{jl}{}^{\lambda}}{\partial m_k}-\frac{V_{jl}{}^{\lambda}}{V_{jl}{}^{2}}\frac{\partial V_{jl}{}^{\mu}}{\partial m_k}. \tag{B2}$$

The partial derivatives appearing in equations (B1) and (B2) are then obtained by differentiating equations (3), and are given in the following table.

$$\frac{1}{a}\frac{\partial V_{jl}{}^{\mu}}{\partial\theta_k} = (\delta_{jk}-\delta_{lk})[\omega_k\cos\lambda\cos\theta_k+\omega_k\sin\lambda\sin\theta_k\cos(\mu-\phi_k)]$$

$$\frac{1}{a}\frac{\partial V_{jl}{}^{\mu}}{\partial\phi_k} = (-\delta_{jk}+\delta_{lk})\,\omega_k\sin\lambda\cos\theta_k\sin(\mu-\phi_k)$$

$$\frac{1}{a}\frac{\partial V_{jl}{}^{\mu}}{\partial\omega_k} = (\delta_{jk}-\delta_{lk})[\cos\lambda\sin\theta_k-\sin\lambda\cos\theta_k\cos(\mu-\phi_k)]$$

$$\frac{1}{a}\frac{\partial V_{jl}^{\lambda}}{\partial \theta_k} = (-\delta_{jk}+\delta_{lk})\,\omega_k \sin\theta_k \sin(\mu-\phi_k)$$

$$\frac{1}{a}\frac{\partial V_{jl}^{\lambda}}{\partial \phi_k} = (-\delta_{jk}+\delta_{lk})\,\omega_k \cos\theta_k \cos(\mu-\phi_k)$$

$$\frac{1}{a}\frac{\partial V_{jl}^{\lambda}}{\partial \omega_k} = (\delta_{jk}-\delta_{lk}) \cos\theta_k \sin(\mu-\phi_k)$$

Here δ_{jk}, δ_{lk}, are Kronecker deltas.